Available online at www.sciencedirect.com
SCIENCE DIRECT®
Journal of Computational Physics 195 (2004) 236–262
JOURNAL OF COMPUTATIONAL PHYSICS
www.elsevier.com/locate/jcp

Iterative forward and inverse algorithms based on domain integral equations for three-dimensional electric and magnetic objects

Aria Abubakar [a,*], Peter M. van den Berg [b]

[a] Schlumberger-Doll Research, 36 Old Quarry Road, Ridgefield, CT 06877-4108, USA
[b] Faculty of Applied Physics, Delft University of Technology, Lorentzweg 1, 2628 CJ, Delft, Netherlands

Received 27 November 2002; received in revised form 23 July 2003; accepted 3 October 2003

Abstract

An iterative approach to full vector three-dimensional inverse scattering problems, where the unknown objects can have conductivity, permittivity and permeability different from the known background medium, is discussed. Since this problem involves a large number of unknowns, it has to be solved effectively and efficiently so that the results can be obtained in timely manner. The forward modeling is based on a domain integral equation approach formulated in terms of the electric and magnetic contrast sources normalized with the characteristic impedance of the background medium. Our numerical tests indicate that this formulation is prerequisite in order to arrive at a forward solution within an acceptable number of iterations, and hence it is also of significant importance in the optimization process of the inverse problem. The inverse scattering problem is attacked using the Multiplicative Regularized Contrast Source Inversion method as known in the literature. The complexity of this inverse method is approximately equal to the complexity of two equivalent forward algorithms of the conjugate gradient type. Furthermore, this inverse method has been armed with a weighted L_2-norm regularizer which has been included as a multiplicative constraint. Some representative numerical testings will be presented to illustrate the ability of the our numerical algorithms.

Keywords: Inverse scattering; Three-dimensional; Full-vectorial; Iterative technique; Nonlinear problem; Integral equation; Electric and magnetic objects

1. Introduction

Two- and three-dimensional electromagnetic inverse scattering problem have been studied with various optimization methods, in particular, deterministic gradient type methods. Among the huge amount of literature we only list a few without intention of review: Abubakar and co-authors [2–7,9,30], Barkeshli and

* Corresponding author. Tel.: +1-203-431-5559; fax: +1-203-438-3819.
E-mail addresses: aabubakar@ridgefield.oilfield.slb.com, aabubakar@slb.com (A. Abubakar).

0021-9991/$ - see front matter © 2003 Elsevier Inc. All rights reserved.
doi:10.1016/j.jcp.2003.10.009

Lautzenheiser [10], Chew and Wang [13], Franchois and Pichot [14], Habashy and co-authors [15,16,27], Isernia et al. [18], Kleinman and van den Berg [19], Liu and co-authors [20,36], Zhdanov and Hursan [33]. Furthermore, a more recent development on the three-dimensional electromagnetic forward and inverse modeling for geophysical applications can be found in [22,34]. All the authors mentioned above handle only one type of material contrast either electric (conductivity and permittivity) or magnetic (permeability). There is some work by Gustafsson and He [28] and by Rekanos [24,25] which addresses the simultaneous reconstruction of the electric and magnetic contrast, but these authors limit themselves to the two-dimensional case.

In this paper we present an inversion method which can be used to invert the electric and magnetic contrast of a three-dimensional object, using a full vectorial formulation. Furthermore, unlike in [24,25,28], we attack the problem using an integral equation approach, which allows one to restrict the computational domain. This will reduce the number of unknowns. In order to be able to arrive at reconstruction results within reasonable computational time, we employ the so-called Contrast Source Inversion (CSI) method [29]. In this CSI method, the unknown contrast sources (the internal fields multiplied by the material contrasts) and the unknown contrasts are reconstructed by minimization of a cost functional. This cost functional is the weighted sum of the error norm in the match of the model (integral representation) to the data and the error norm in satisfying of the integral equation inside the domain of interest. Earlier, Zhdanov and Chernyak [32] have proposed an inversion scheme based on an (unweighted) sum of these error norms, but ample experience has shown that the proper weighting is essential to the success of the CSI method and its application to the present problem. Subsequently, the minimization procedure is carried in two alternate steps: (1) the contrast sources are updated via a conjugate gradient direction of the cost functional; (2) the contrasts are found by direct minimization of the appropriate terms in the cost functional which is equivalent to find the least-square fit of the constitutive relations between the contrast sources and the fields. In this way the total complexity of each iteration in the CSI method is approximately equal to the complexity of two iterations of the Conjugate Gradient method of the equivalent forward problem. This is one of the reasons which allow us to attack a full vectorial three-dimensional electromagnetic inverse problem with contrast in conductivity, permittivity and permeability.

When the number of data is very limited and a significant noise level is present in the data, which is always the case in our application, the CSI method will not provide one with a reasonable resolution of the reconstruction results. Furthermore, the question is how to restore the band limitation of the images we have obtained with the Contrast Source Inversion method. In image processing, there are a number of methods to enhance an image by minimization the variation of the contrast which is equivalent by providing some a priori information. Our strategy is to combine one and another by minimization of the total variation of the contrast, during the whole inversion process. The standard way is to include such a norm in the cost functional by introducing an extra penalty function. Although the addition of this extra regularizer to the cost functional has a very positive effect on the quality of the reconstruction for both 'blocky' and smooth profiles, a drawback is the presence of a weighting parameter in the cost functional, which can only be determined through considerable numerical experimentation, especially for our present case which is a problem that requires extensive computational forces.

Although there are many practical ways of determining the optimal regularization parameter in the framework of Tikhonov regularization (see e.g. [35]), one of the most simple techniques is the so-called adaptive regularization with progressively decreasing regularization parameter. This has led to the idea of including the total variation as a multiplicative constraint [8,31], with the result that the original cost functional is the weighting parameter of the regularizer, so that this parameter is determined by the inversion procedure itself. It appears to be very effective, without major a priori information about the shape and the constitution of the object configuration. This makes the algorithm suitable to invert experimental data 'blindly' as shown in by Bloemenkamp et al. [12]. Later on, the CSI method based on a new weighted L^2-norm regularizer [30,31] is used in stead of the standard total variation applied to handle complicated

biological objects embedded in a lossy medium for both the two- and three-dimensional cases [9]. This weighted L_2-norm regularizer provides significant improvement compared to its predecessor, the L_1-norm Total Variation, since it allows us to find all the updating parameters for the contrast in closed-form. Further, although one may argue that by including the regularizer as a multiplicative factor, the nonlinearity of the problem is increased, a careful analysis shows that, under certain restrictions, no new local minima are introduced using this multiplicative technique with the weighted L^2-norm as regularization factor. Hence, in the work reported in this paper we will employ the CSI method using the weighted L_2-norm regularizer as our inversion scheme. This method is denoted as Multiplicative Regularized CSI method (MR-CSI). Numerical examples using simulated data are presented to demonstrate the capabilities of the MR-CSI method.

2. Integral representations

We assume the scatterer with support D^{sct}, to be located in a homogeneous background medium with permittivity ε_{b}, conductivity σ_{b} and permeability μ_{b}. We define a computational domain D, such that $D^{\text{sct}} \in D$. A Cartesian coordinate system is centered in D with spatial points denoted by $\boldsymbol{x} = (x_1, x_2, x_3)$. The excitation source can be either a magnetic or electric dipole depending on the application at hand. The sources and receivers are assumed to be located in S, outside D.

The fields are assumed to be vary sinusoidally with time t with frequency ω, with time factor $\exp(-\mathrm{i}\omega t)$ where $\mathrm{i}^2 = -1$. The corresponding wavelength is denoted by λ. If the vector $\boldsymbol{E}^{\text{inc}}$ and $\boldsymbol{H}^{\text{inc}}$ denote the incident fields excited by either electric or magnetic sources, then the total fields in D are given by

$$\boldsymbol{E}(\boldsymbol{x}) = \boldsymbol{E}^{\text{inc}}(\boldsymbol{x}) + \boldsymbol{E}^{\text{sct}}(\boldsymbol{x}) \quad \text{and} \quad \boldsymbol{H}(\boldsymbol{x}) = \boldsymbol{H}^{\text{inc}}(\boldsymbol{x}) + \boldsymbol{H}^{\text{sct}}(\boldsymbol{x}), \tag{1}$$

where $\boldsymbol{E}^{\text{sct}}$ and $\boldsymbol{H}^{\text{sct}}$ denote the scattered fields. In (1), the symbol $\boldsymbol{E}$ stands for the electric field and the symbol $\boldsymbol{H}$ stands for the magnetic field. It is well known that the total field in D satisfies the following domain integral equations [17]:

$$\begin{aligned}\boldsymbol{E}^{\text{inc}}(\boldsymbol{x}) = \boldsymbol{E}(\boldsymbol{x}) &- [k_{\text{b}}^2 + \boldsymbol{\nabla}\boldsymbol{\nabla}\cdot] \int_D g(\boldsymbol{x}-\boldsymbol{x}')\chi^{\text{E}}(\boldsymbol{x}')\boldsymbol{E}(\boldsymbol{x}') \, \mathrm{d}v(\boldsymbol{x}') \\ &- \mathrm{i}\omega\mu_{\text{b}}\boldsymbol{\nabla} \times \int_D g(\boldsymbol{x}-\boldsymbol{x}')\chi^{\text{H}}(\boldsymbol{x}')\boldsymbol{H}(\boldsymbol{x}') \, \mathrm{d}v(\boldsymbol{x}'),\end{aligned} \tag{2}$$

$$\begin{aligned}\boldsymbol{H}^{\text{inc}}(\boldsymbol{x}) = \boldsymbol{H}(\boldsymbol{x}) &- \sigma'_{\text{b}}\boldsymbol{\nabla} \times \int_D g(\boldsymbol{x}-\boldsymbol{x}')\chi^{\text{E}}(\boldsymbol{x}')\boldsymbol{E}(\boldsymbol{x}') \, \mathrm{d}v(\boldsymbol{x}') \\ &- [k_{\text{b}}^2 + \boldsymbol{\nabla}\boldsymbol{\nabla}\cdot] \int_D g(\boldsymbol{x}-\boldsymbol{x}')\chi^{\text{H}}(\boldsymbol{x}')\boldsymbol{H}(\boldsymbol{x}') \, \mathrm{d}v(\boldsymbol{x}'),\end{aligned} \tag{3}$$

where the electric contrast χ^{E} and the magnetic contrast χ^{H} are given by

$$\chi^{\text{E}}(\boldsymbol{x}) = \frac{\sigma'(\boldsymbol{x})}{\sigma'_{\text{b}}} - 1 \quad \text{and} \quad \chi^{\text{H}}(\boldsymbol{x}) = \frac{\mu(\boldsymbol{x})}{\mu_{\text{b}}} - 1, \tag{4}$$

in which

$$\sigma'(\boldsymbol{x}) = \sigma(\boldsymbol{x}) - \mathrm{i}\omega\varepsilon(\boldsymbol{x}) \quad \text{and} \quad \sigma'_{\text{b}} = \sigma_{\text{b}} - \mathrm{i}\omega\varepsilon_{\text{b}}. \tag{5}$$

In (4) and (5), $\varepsilon(\boldsymbol{x})$ is the permittivity, $\sigma(\boldsymbol{x})$ is the conductivity and $\mu(\boldsymbol{x})$ is the permeability of the contrasting domain D. Note that if we consider a low-frequency electromagnetic measurement (in the so-called diffusive

range), the terms containing the permittivities in (5) can be neglected. Then $\sigma' = \sigma$ is real and positive. In (2) and (3), the symbol $\nabla = (\partial_1, \partial_2, \partial_3)$ denotes the spatial differentiation with respect to the position vector $\boldsymbol{x} = (x_1, x_2, x_3)$ and the homogeneous scalar Green function g is given by

$$g(\boldsymbol{x}) = \frac{\exp(\mathrm{i}k_\mathrm{b}|\boldsymbol{x}|)}{4\pi|\boldsymbol{x}|}, \quad \text{with } k_\mathrm{b} = (\mathrm{i}\omega\mu_\mathrm{b}\sigma'_\mathrm{b})^{\frac{1}{2}},\ \mathrm{Re}(k_\mathrm{b}) > 0. \tag{6}$$

We observe that in the integrand of (2) and (3) the fields and the contrasts occur as products terms. Hence, for our forward and inverse models we propose to take these so-called contrast sources as the fundamental unknowns, defined by

$$\boldsymbol{W}^\mathrm{E}(\boldsymbol{x}) = \chi^\mathrm{E}(\boldsymbol{x})\boldsymbol{E}(\boldsymbol{x}) \quad \text{and} \quad \boldsymbol{W}^\mathrm{H}(\boldsymbol{x}) = \chi^\mathrm{H}(\boldsymbol{x})\boldsymbol{H}(\boldsymbol{x}). \tag{7}$$

Multiplying (2) with the electric contrast χ^E and (3) with the magnetic contrast χ^H and using (7), we obtain

$$\begin{aligned}\chi^\mathrm{E}(\boldsymbol{x})\boldsymbol{E}^\mathrm{inc}(\boldsymbol{x}) = {} & \boldsymbol{W}^\mathrm{E}(\boldsymbol{x}) - \chi^\mathrm{E}(\boldsymbol{x})[k_\mathrm{b}^2 + \nabla\nabla\cdot] \int_D g(\boldsymbol{x}-\boldsymbol{x}')\boldsymbol{W}^\mathrm{E}(\boldsymbol{x}')\,\mathrm{d}v(\boldsymbol{x}') \\ & - \chi^\mathrm{E}(\boldsymbol{x})\mathrm{i}\omega\mu_\mathrm{b}\nabla\times \int_D g(\boldsymbol{x}-\boldsymbol{x}')\boldsymbol{W}^\mathrm{H}(\boldsymbol{x}')\,\mathrm{d}v(\boldsymbol{x}'),\end{aligned} \tag{8}$$

$$\begin{aligned}\chi^\mathrm{H}(\boldsymbol{x})\boldsymbol{H}^\mathrm{inc}(\boldsymbol{x}) = {} & \boldsymbol{W}^\mathrm{H}(\boldsymbol{x}) - \chi^\mathrm{H}(\boldsymbol{x})\sigma'_\mathrm{b}\nabla\times \int_D g(\boldsymbol{x}-\boldsymbol{x}')\boldsymbol{W}^\mathrm{E}(\boldsymbol{x}')\,\mathrm{d}v(\boldsymbol{x}') \\ & - \chi^\mathrm{H}(\boldsymbol{x})[k_\mathrm{b}^2 + \nabla\nabla\cdot] \int_D g(\boldsymbol{x}-\boldsymbol{x}')\boldsymbol{W}^\mathrm{H}(\boldsymbol{x}')\,\mathrm{d}v(\boldsymbol{x}').\end{aligned} \tag{9}$$

The advantage of the use of these domain integral equations is the fact that the contrast functions χ^E and χ^H occur outside the integral operators and that these integral operators are convolutions in space. Furthermore, we observe that for given contrast sources $\boldsymbol{W}^\mathrm{E}$ and $\boldsymbol{W}^\mathrm{H}$, the electric contrast χ^E follows from (8) only, while the magnetic contrast χ^H follows from (9) only. This observation leads to significant simplifications in the development of our algorithm for the inverse scattering problem.

We further note that the values of the electric and magnetic fields (hence also the electric and magnetic contrast sources) can significantly differ in order. To avoid any numerical difficulty, we propose to work with renormalized integral equations as follows:

$$\begin{aligned}\chi^\mathrm{E}(\boldsymbol{x})\boldsymbol{E}^\mathrm{inc}(\boldsymbol{x}) = {} & \boldsymbol{w}^\mathrm{E}(\boldsymbol{x}) - \chi^\mathrm{E}(\boldsymbol{x})[k_\mathrm{b}^2 + \nabla\nabla\cdot] \int_D g(\boldsymbol{x}-\boldsymbol{x}')\boldsymbol{w}^\mathrm{E}(\boldsymbol{x}')\,\mathrm{d}v(\boldsymbol{x}') \\ & - \chi^\mathrm{E}(\boldsymbol{x})\frac{\mathrm{i}\omega\mu_\mathrm{b}}{Z_\mathrm{b}}\nabla\times \int_D g(\boldsymbol{x}-\boldsymbol{x}')\boldsymbol{w}^\mathrm{H}(\boldsymbol{x}')\,\mathrm{d}v(\boldsymbol{x}'),\end{aligned} \tag{10}$$

$$\begin{aligned}\chi^\mathrm{H}(\boldsymbol{x})Z_\mathrm{b}\boldsymbol{H}^\mathrm{inc}(\boldsymbol{x}) = {} & \boldsymbol{w}^\mathrm{H}(\boldsymbol{x}) - \chi^\mathrm{H}(\boldsymbol{x})Z_\mathrm{b}\sigma'_\mathrm{b}\nabla\times \int_D g(\boldsymbol{x}-\boldsymbol{x}')\boldsymbol{w}^\mathrm{E}(\boldsymbol{x}')\,\mathrm{d}v(\boldsymbol{x}') \\ & - \chi^\mathrm{H}(\boldsymbol{x})[k_\mathrm{b}^2 + \nabla\nabla\cdot] \int_D g(\boldsymbol{x}-\boldsymbol{x}')\boldsymbol{w}^\mathrm{H}(\boldsymbol{x}')\,\mathrm{d}v(\boldsymbol{x}'),\end{aligned} \tag{11}$$

where Z_b is the characteristic impedance of the background medium,

$$Z_\mathrm{b} = \left(\frac{-\mathrm{i}\omega\mu_\mathrm{b}}{\sigma'_\mathrm{b}}\right)^{\frac{1}{2}} = \left(\frac{-k_\mathrm{b}^2}{\sigma_\mathrm{b}'^2}\right)^{\frac{1}{2}}, \tag{12}$$

and where the normalized contrast sources are introduced as

$$\boldsymbol{w}^{\mathrm{E}}(\boldsymbol{x}) = \boldsymbol{W}^{\mathrm{E}}(\boldsymbol{x}) \quad \text{and} \quad \boldsymbol{w}^{\mathrm{H}}(\boldsymbol{x}) = Z_{\mathrm{b}}\boldsymbol{W}^{\mathrm{H}}(\boldsymbol{x}). \tag{13}$$

Once the electric and magnetic contrast sources vectors in D are known, the scattered fields at the observation domain S can be computed through:

$$\boldsymbol{E}^{\mathrm{sct}}(\boldsymbol{x}) = \int_D (k_{\mathrm{b}}^2 + \boldsymbol{\nabla}'\boldsymbol{\nabla}'\cdot)g(\boldsymbol{x}-\boldsymbol{x}')\boldsymbol{w}^{\mathrm{E}}(\boldsymbol{x}')\,\mathrm{d}v(\boldsymbol{x}') + \int_D \frac{-\mathrm{i}\omega\mu_{\mathrm{b}}}{Z_{\mathrm{b}}}\boldsymbol{\nabla}'g(\boldsymbol{x}-\boldsymbol{x}')\times\boldsymbol{w}^{\mathrm{H}}(\boldsymbol{x}')\,\mathrm{d}v(\boldsymbol{x}'), \tag{14}$$

$$\boldsymbol{H}^{\mathrm{sct}}(\boldsymbol{x}) = -\int_D \sigma_{\mathrm{b}}'\boldsymbol{\nabla}'g(\boldsymbol{x}-\boldsymbol{x}')\times\boldsymbol{w}^{\mathrm{E}}(\boldsymbol{x}')\,\mathrm{d}v(\boldsymbol{x}') + \int_D \frac{1}{Z_{\mathrm{b}}}(k_{\mathrm{b}}^2 + \boldsymbol{\nabla}'\boldsymbol{\nabla}'\cdot)g(\boldsymbol{x}-\boldsymbol{x}')\boldsymbol{w}^{\mathrm{H}}(\boldsymbol{x}')\,\mathrm{d}v(\boldsymbol{x}'), \tag{15}$$

where $\boldsymbol{\nabla}' = (\partial_1', \partial_2', \partial_3')$ denotes spatial differentiation with respect to $\boldsymbol{x}' = (x_1, x_2, x_3)$.

From a physical point of view, the integral representations (14) and (15) show that the scattered field is generated by excess electric and magnetic currents flowing in a homogeneous embedding within the contrasting object, while (10) and (11) are the equations from which these excess electric and magnetic currents can be solved. The latter equations are singular integral equations, in which grad-div and curl operators act on normalized vector potentials, defined as the spatial convolutions of the Green function and the contrast sources. Numerical implementation of such integral equations must be carried out carefully.

3. Forward scattering problem

We discretize the object domain D using a mesh uniformly subdivided in the x_1, x_2, and x_3 direction with spacing Δx_1, Δx_2, and Δx_3, respectively. In each rectangular subdomain, we assume the contrast sources and the contrasts to be constant. The integral operators are discretized by first applying the weakening procedure in order to cope with the singularity nature of the integral equations. After that all spatial differentiations are calculated using the finite difference rule. This discretization technique has been proven accurate and efficient for different type of integral equations (see [2] for the static case and see [6,37,38] for the diffusive and wavefield cases). In Appendix A, we present the discretized version of the domain integral equations for the electric and magnetic contrast sources.

After discretization, we obtain a linear system of equations for $w^{\mathrm{E}}_{\kappa;m,n,p}$ and $w^{\mathrm{H}}_{\kappa;m,n,p}$ when both $\chi^{\mathrm{E}}_{m,n,p}$ and $\chi^{\mathrm{H}}_{m,n,p}$ are known. Here the subscript κ denotes the components of a vector and while m, n and p denote the discrete values at the different points of observation in the object domain D. This linear system of equations can be written compactly in operator notations as

$$\chi^{\mathrm{E}}\boldsymbol{E}^{\mathrm{inc}} = \mathscr{L}_D^{\mathrm{EE}}\boldsymbol{w}^{\mathrm{E}} + \mathscr{L}_D^{\mathrm{EH}}\boldsymbol{w}^{\mathrm{H}}, \tag{16}$$

$$\chi^{\mathrm{H}}Z_{\mathrm{b}}\boldsymbol{H}^{\mathrm{inc}} = \mathscr{L}_D^{\mathrm{HE}}\boldsymbol{w}^{\mathrm{E}} + \mathscr{L}_D^{\mathrm{HH}}\boldsymbol{w}^{\mathrm{H}}, \tag{17}$$

where the operators are defined as

$$(\mathscr{L}_D^{\mathrm{EE}}\boldsymbol{w}^{\mathrm{E}} + \mathscr{L}_D^{\mathrm{EH}}\boldsymbol{w}^{\mathrm{H}})_{\kappa;m,n,p} = w^{\mathrm{E}}_{\kappa;m,n,p} - \chi^{\mathrm{E}}_{m,n,p}(k_{\mathrm{b}}^2 A^{\mathrm{E}}_{\kappa;m,n,p} + B^{\mathrm{E}}_{\kappa;m,n,p}), \tag{18}$$

$$(\mathscr{L}_D^{\mathrm{HE}}\boldsymbol{w}^{\mathrm{E}} + \mathscr{L}_D^{\mathrm{HH}}\boldsymbol{w}^{\mathrm{H}})_{\kappa;m,n,p} = w^{\mathrm{H}}_{\kappa;m,n,p} - \chi^{\mathrm{H}}_{m,n,p}(k_{\mathrm{b}}^2 A^{\mathrm{H}}_{\kappa;m,n,p} + B^{\mathrm{H}}_{\kappa;m,n,p}) \tag{19}$$

for $\kappa = 1,2,3$, $m = 1,\ldots,M$, $n = 1,\ldots,N$, $p = 1,\ldots,P$ and where $B^{\mathrm{E}}_{\kappa;m,n,p}$, $B^{\mathrm{H}}_{\kappa;m,n,p}$, $A^{\mathrm{E}}_{\kappa;m,n,p}$ and $A^{\mathrm{H}}_{\kappa;m,n,p}$ are given in (A.10)–(A.12).

Since all the expressions of $B^{\mathrm{E}}_{\kappa;m,n,p}$, $B^{\mathrm{H}}_{\kappa;m,n,p}$, $A^{\mathrm{E}}_{\kappa;m,n,p}$ and $A^{\mathrm{H}}_{\kappa;m,n,p}$ consist of spatial convolutions in space, we can advantageously use Fast Fourier Transform (FFT) routines to compute them. However, we then need

an iterative solution, and the Conjugate Gradient (CG) method seems to be one of the most efficient methods. With this so-called CG-FFT technique we are able to solve complex three-dimensional problems efficiently. Furthermore, it also gives the fundament of our solution for the inverse modeling.

3.1. Algorithm

This combination of the CG type method and the FFT algorithm has been used extensively for the integral equation either for the electric contrast only or magnetic contrast only, see [2,6,20,21,36–38]. Although there are a number of algorithms which can take into account an object with the electric and magnetic contrasts simultaneously, they are all (to our knowledge) based on local equations (finite difference types) and handle two-dimensional cases only, see [25,28]. In the present work we have to deal with both electric and magnetic contrast source vectors and we consider the full three-dimensional case. This complicates significantly the problem. Using matrix notations the domain integral equations in (16)–(19) can be written as

$$\begin{bmatrix} \chi^{\mathrm{E}}\boldsymbol{E}^{\mathrm{inc}} \\ \chi^{\mathrm{H}}Z_{\mathrm{b}}\boldsymbol{H}^{\mathrm{inc}} \end{bmatrix} = \begin{bmatrix} \mathscr{L}_D^{\mathrm{EE}} & \mathscr{L}_D^{\mathrm{EH}} \\ \mathscr{L}_D^{\mathrm{HE}} & \mathscr{L}_D^{\mathrm{HH}} \end{bmatrix} \begin{bmatrix} \boldsymbol{w}^{\mathrm{E}} \\ \boldsymbol{w}^{\mathrm{H}} \end{bmatrix}. \tag{20}$$

We observe that the matrix describing this linear system of equations is non-symmetric. Therefore, we also need the adjoint operator in order to set up a CG scheme. In such a scheme we also need the definition of the norm and the inner product. In view of the definition of the discretized field quantities, the square norm (the inner product) on domain D of two vector function on D is given by

$$\langle \boldsymbol{u}, \boldsymbol{v} \rangle_D = \Delta x_1 \Delta x_2 \Delta x_3 \sum_{m=1}^{M} \sum_{n=1}^{N} \sum_{p=1}^{P} \boldsymbol{u}_{m,n,p} \cdot \overline{\boldsymbol{v}}_{m,n,p}, \tag{21}$$

where the overbar denotes the complex conjugate and the dot $(\cdot)$ denotes the dot product of two vector functions. The adjoint operators are defined via

$$\left\langle \begin{bmatrix} \boldsymbol{r}^{\mathrm{E}} \\ \boldsymbol{r}^{\mathrm{H}} \end{bmatrix}, \begin{bmatrix} \mathscr{L}_D^{\mathrm{EE}} & \mathscr{L}_D^{\mathrm{EH}} \\ \mathscr{L}_D^{\mathrm{HE}} & \mathscr{L}_D^{\mathrm{HH}} \end{bmatrix} \begin{bmatrix} \boldsymbol{w}^{\mathrm{E}} \\ \boldsymbol{w}^{\mathrm{H}} \end{bmatrix} \right\rangle_D = \left\langle \begin{bmatrix} \mathscr{L}^{\mathrm{EE}*} & \mathscr{L}^{\mathrm{HE}*} \\ \mathscr{L}^{\mathrm{EH}*} & \mathscr{L}^{\mathrm{HH}*} \end{bmatrix} \begin{bmatrix} \boldsymbol{r}^{\mathrm{E}} \\ \boldsymbol{r}^{\mathrm{H}} \end{bmatrix}, \begin{bmatrix} \boldsymbol{w}^{\mathrm{E}} \\ \boldsymbol{w}^{\mathrm{H}} \end{bmatrix} \right\rangle_D. \tag{22}$$

The discretized form of this adjoint operators $\mathscr{L}^{\mathrm{EE}*}$, $\mathscr{L}^{\mathrm{EH}*}$, $\mathscr{L}^{\mathrm{HE}*}$ and $\mathscr{L}^{\mathrm{HH}*}$ are given in Appendix B.

With these definitions we now formulate the CG scheme that minimizes iteratively the error norm

$$F_D(\boldsymbol{w}^{\mathrm{E}}, \boldsymbol{w}^{\mathrm{H}}) = \eta_D^{\mathrm{E}} \left\| \chi^{\mathrm{E}}\boldsymbol{E}^{\mathrm{inc}} - \mathscr{L}_D^{\mathrm{EE}}\boldsymbol{w}^{\mathrm{E}} - \mathscr{L}_D^{\mathrm{EH}}\boldsymbol{w}^{\mathrm{H}} \right\|_D^2 + \eta_D^{\mathrm{H}} \left\| \chi^{\mathrm{H}}Z_{\mathrm{b}}\boldsymbol{H}^{\mathrm{inc}} - \mathscr{L}_D^{\mathrm{HE}}\boldsymbol{w}^{\mathrm{E}} - \mathscr{L}_D^{\mathrm{HH}}\boldsymbol{w}^{\mathrm{H}} \right\|_D^2, \tag{23}$$

where the normalization factors are given by

$$\eta_D^{\mathrm{E}} = \left\| \chi^{\mathrm{E}}\boldsymbol{E}^{\mathrm{inc}} \right\|_D^{-2} \quad \text{and} \quad \eta_D^{\mathrm{H}} = \left\| \chi^{\mathrm{H}}Z_{\mathrm{b}}\boldsymbol{H}^{\mathrm{inc}} \right\|_D^{-2}. \tag{24}$$

We start the CG scheme with zero initial estimates $[\boldsymbol{w}_0^{\mathrm{E}} \ \ \boldsymbol{w}_0^{\mathrm{H}}] = [\boldsymbol{0} \ \ \boldsymbol{0}]$. Then it computes

$$\begin{bmatrix} \boldsymbol{v}_1^{\mathrm{E}} \\ \boldsymbol{v}_1^{\mathrm{H}} \end{bmatrix} = \begin{bmatrix} \boldsymbol{g}_1^{\mathrm{E}} \\ \boldsymbol{g}_1^{\mathrm{H}} \end{bmatrix} = \begin{bmatrix} \eta_D^{\mathrm{E}}\mathscr{L}_D^{\mathrm{EE}*} & \eta_D^{\mathrm{H}}\mathscr{L}_D^{\mathrm{HE}*} \\ \eta_D^{\mathrm{E}}\mathscr{L}_D^{\mathrm{EH}*} & \eta_D^{\mathrm{H}}\mathscr{L}_D^{\mathrm{HH}*} \end{bmatrix} \begin{bmatrix} \chi^{\mathrm{E}}\boldsymbol{E}^{\mathrm{inc}} \\ \chi^{\mathrm{H}}Z_{\mathrm{b}}\boldsymbol{H}^{\mathrm{inc}} \end{bmatrix}, \tag{25}$$

$$\begin{bmatrix} \boldsymbol{w}_1^{\mathrm{E}} \\ \boldsymbol{w}_1^{\mathrm{H}} \end{bmatrix} = \frac{\|\boldsymbol{g}_1^{\mathrm{E}}\|_D^2 + \|\boldsymbol{g}_1^{\mathrm{H}}\|_D^2}{\|\mathscr{L}_D^{\mathrm{EE}}\boldsymbol{g}_1^{\mathrm{E}} + \mathscr{L}_D^{\mathrm{EH}}\boldsymbol{g}_1^{\mathrm{H}}\|_D^2 + \|\mathscr{L}_D^{\mathrm{HE}}\boldsymbol{g}_1^{\mathrm{E}} + \mathscr{L}_D^{\mathrm{HH}}\boldsymbol{g}_1^{\mathrm{H}}\|_D^2} \begin{bmatrix} \boldsymbol{g}_1^{\mathrm{E}} \\ \boldsymbol{g}_1^{\mathrm{H}} \end{bmatrix}, \tag{26}$$

with resulting residual errors

$$\begin{bmatrix} \boldsymbol{r}_1^{\mathrm{E}} \\ \boldsymbol{r}_1^{\mathrm{H}} \end{bmatrix} = \begin{bmatrix} \chi^{\mathrm{E}} \boldsymbol{E}^{\mathrm{inc}} \\ \chi^{\mathrm{H}} Z_{\mathrm{b}} \boldsymbol{H}^{\mathrm{inc}} \end{bmatrix} - \begin{bmatrix} \mathscr{L}_D^{\mathrm{EE}} & \mathscr{L}_D^{\mathrm{EH}} \\ \mathscr{L}_D^{\mathrm{HE}} & \mathscr{L}_D^{\mathrm{HH}} \end{bmatrix} \begin{bmatrix} \boldsymbol{w}_1^{\mathrm{E}} \\ \boldsymbol{w}_1^{\mathrm{H}} \end{bmatrix}, \tag{27}$$

and computes successively for $n = 2, 3, \ldots,$

$$\begin{bmatrix} \boldsymbol{g}_n^{\mathrm{E}} \\ \boldsymbol{g}_n^{\mathrm{H}} \end{bmatrix} = \begin{bmatrix} \eta_D^{\mathrm{E}} \mathscr{L}_D^{\mathrm{EE}*} & \eta_D^{\mathrm{H}} \mathscr{L}_D^{\mathrm{HE}*} \\ \eta_D^{\mathrm{E}} \mathscr{L}_D^{\mathrm{EH}*} & \eta_D^{\mathrm{H}} \mathscr{L}_D^{\mathrm{HH}*} \end{bmatrix} \begin{bmatrix} \boldsymbol{r}_{n-1}^{\mathrm{E}} \\ \boldsymbol{r}_{n-1}^{\mathrm{H}} \end{bmatrix}, \tag{28}$$

$$\begin{bmatrix} \boldsymbol{v}_n^{\mathrm{E}} \\ \boldsymbol{v}_n^{\mathrm{H}} \end{bmatrix} = \begin{bmatrix} \boldsymbol{g}_n^{\mathrm{E}} \\ \boldsymbol{g}_n^{\mathrm{H}} \end{bmatrix} + \gamma_n \begin{bmatrix} \boldsymbol{v}_{n-1}^{\mathrm{E}} \\ \boldsymbol{v}_{n-1}^{\mathrm{H}} \end{bmatrix}, \quad \gamma_n = \frac{\|\boldsymbol{g}_n^{\mathrm{E}}\|_D^2 + \|\boldsymbol{g}_n^{\mathrm{H}}\|_D^2}{\|\boldsymbol{g}_{n-1}^{\mathrm{E}}\|_D^2 + \|\boldsymbol{g}_{n-1}^{\mathrm{H}}\|_D^2}, \tag{29}$$

$$\begin{bmatrix} \boldsymbol{w}_n^{\mathrm{E}} \\ \boldsymbol{w}_n^{\mathrm{H}} \end{bmatrix} = \begin{bmatrix} \boldsymbol{w}_{n-1}^{\mathrm{E}} \\ \boldsymbol{w}_{n-1}^{\mathrm{H}} \end{bmatrix} + \frac{\langle \boldsymbol{g}_n^{\mathrm{E}}, \boldsymbol{v}_n^{\mathrm{E}} \rangle_D + \langle \boldsymbol{g}_n^{\mathrm{H}}, \boldsymbol{v}_n^{\mathrm{H}} \rangle_D}{\|\mathscr{L}_D^{\mathrm{EE}} \boldsymbol{v}_n^{\mathrm{E}} + \mathscr{L}_D^{\mathrm{EH}} \boldsymbol{v}_n^{\mathrm{H}}\|_D^2 + \|\mathscr{L}_D^{\mathrm{HE}} \boldsymbol{v}_n^{\mathrm{E}} + \mathscr{L}_D^{\mathrm{HH}} \boldsymbol{v}_n^{\mathrm{H}}\|_D^2} \begin{bmatrix} \boldsymbol{v}_n^{\mathrm{E}} \\ \boldsymbol{v}_n^{\mathrm{H}} \end{bmatrix}, \tag{30}$$

with resulting residual errors

$$\begin{bmatrix} \boldsymbol{r}_n^{\mathrm{E}} \\ \boldsymbol{r}_n^{\mathrm{H}} \end{bmatrix} = \begin{bmatrix} \chi^{\mathrm{E}} \boldsymbol{E}^{\mathrm{inc}} \\ \chi^{\mathrm{H}} Z_{\mathrm{b}} \boldsymbol{H}^{\mathrm{inc}} \end{bmatrix} - \begin{bmatrix} \mathscr{L}_D^{\mathrm{EE}} & \mathscr{L}_D^{\mathrm{EH}} \\ \mathscr{L}_D^{\mathrm{HE}} & \mathscr{L}_D^{\mathrm{HH}} \end{bmatrix} \begin{bmatrix} \boldsymbol{w}_n^{\mathrm{E}} \\ \boldsymbol{w}_n^{\mathrm{H}} \end{bmatrix}. \tag{31}$$

In fact, this CG scheme solves iteratively the symmetrized system of linear equations:

$$\begin{bmatrix} \eta_D^{\mathrm{E}} \mathscr{L}_D^{\mathrm{EE}*} \mathscr{L}_D^{\mathrm{EE}} & \eta_D^{\mathrm{H}} \mathscr{L}_D^{\mathrm{HE}*} \mathscr{L}_D^{\mathrm{EH}} \\ \eta_D^{\mathrm{E}} \mathscr{L}_D^{\mathrm{EH}*} \mathscr{L}_D^{\mathrm{HE}} & \eta_D^{\mathrm{H}} \mathscr{L}_D^{\mathrm{HH}*} \mathscr{L}_D^{\mathrm{HH}} \end{bmatrix} \begin{bmatrix} \boldsymbol{w}_n^{\mathrm{E}} \\ \boldsymbol{w}_n^{\mathrm{H}} \end{bmatrix} = \begin{bmatrix} \eta_D^{\mathrm{E}} \mathscr{L}_D^{\mathrm{EE}*} \chi^{\mathrm{E}} \boldsymbol{E}^{\mathrm{inc}} + \eta_D^{\mathrm{H}} \mathscr{L}_D^{\mathrm{HE}*} \chi^{\mathrm{H}} Z_{\mathrm{b}} \boldsymbol{H}^{\mathrm{inc}} \\ \eta_D^{\mathrm{E}} \mathscr{L}_D^{\mathrm{EH}*} \chi^{\mathrm{E}} \boldsymbol{E}^{\mathrm{inc}} + \eta_D^{\mathrm{H}} \mathscr{L}_D^{\mathrm{HH}*} \chi^{\mathrm{H}} Z_{\mathrm{b}} \boldsymbol{H}^{\mathrm{inc}} \end{bmatrix}. \tag{32}$$

3.2. Numerical example

Before we proceed with the inverse scattering problem, we first show the advantage of using the domain integral equation formulated in terms of $\boldsymbol{w}^{\mathrm{E}}$ and $\boldsymbol{w}^{\mathrm{H}}$ as given in (10) and (11) above the other two alternatives, namely the one formulated in terms of $\boldsymbol{E}$ and $\boldsymbol{H}$ given in (2) and (3) and in terms of $\boldsymbol{W}^{\mathrm{E}}$ and $\boldsymbol{W}^{\mathrm{H}}$ given in (8) and (9), for two representative numerical examples. We consider the three-dimensional model as shown in Fig. 1. In the object domain D we have two disjointed object O_1 and O_2. The object O_1 with dimension of λ by λ by λ is an object with electric contrast only, $\chi^{\mathrm{E}} = 0.8 + \mathrm{i}0.4$, while the object O_2 with dimension of λ by λ by λ is an object with magnetic contrast only, $\chi^{\mathrm{H}} = 0.8$. These two objects are located in the object (computational) domain D with dimension of 3λ by 3λ by 3λ. The background is vacuum. The computational domain D is subdivided into 30 by 30 by 30 rectangular subdomains. Hence the discretization is 10 points per wavelength which is more than enough to obtain a reliable solution when one uses the integral equation approach [12].

As the excitation source model, we employ a unit point magnetic dipole directed in the positive vertical x_3 direction located at $\boldsymbol{x}^{\mathrm{S}} = (0, -1.6\lambda, 0)$ just outside the object domain D. Hence, the incident fields in the domain D are given by

$$\boldsymbol{E}^{\mathrm{inc}}(\boldsymbol{x}) = -\mathrm{i}\omega\mu_{\mathrm{b}} \big[\partial_2 g(\boldsymbol{x} - \boldsymbol{x}^{\mathrm{S}}) \boldsymbol{i}_1 - \partial_1 g(\boldsymbol{x} - \boldsymbol{x}^{\mathrm{S}}) \boldsymbol{i}_2\big], \tag{33}$$

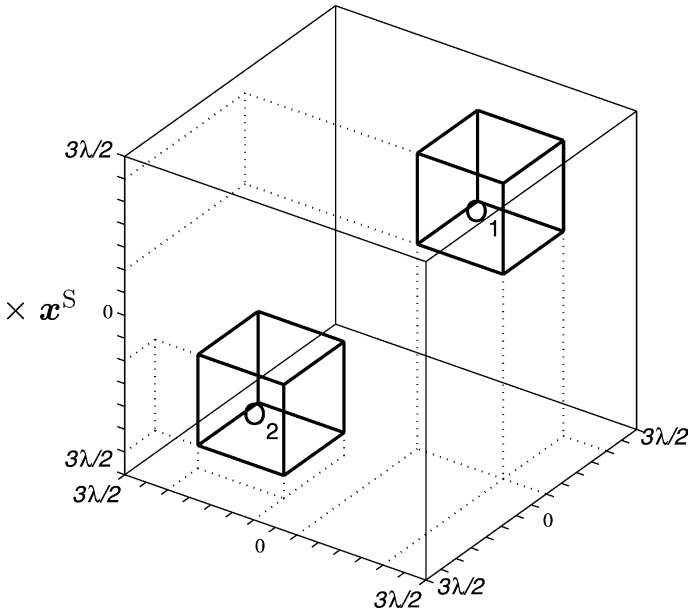

Fig. 1. The rectangular objects O_1 and O_2 in the computational domain D.

$$\boldsymbol{H}^{\mathrm{inc}}(\boldsymbol{x}) = -\left[\partial_3\partial_1 g(\boldsymbol{x}-\boldsymbol{x}^{\mathrm{S}})\boldsymbol{i}_1 + \partial_3\partial_2 g(\boldsymbol{x}-\boldsymbol{x}^{\mathrm{S}})\boldsymbol{i}_2 + \left(k_{\mathrm{b}}^2 + \partial_3^2\right) g(\boldsymbol{x}-\boldsymbol{x}^{\mathrm{S}})\boldsymbol{i}_3\right]. \tag{34}$$

In Fig. 2 we present a convergence rate picture (the square root of the cost functional of (23) plotted against the number of iterations) of the CG methods using the field formulations $\boldsymbol{E}$ and $\boldsymbol{H}$ (see dashed-dotted line), using the contrast sources formulations $\boldsymbol{W}^{\mathrm{E}}$ and $\boldsymbol{W}^{\mathrm{H}}$ (see dashed line) and using the normalized contrast sources formulations $\boldsymbol{w}^{\mathrm{E}}$ and $\boldsymbol{w}^{\mathrm{H}}$ (see solid line). From the results, it is obvious that we will proceed with the normalized contrast source formulations. If we investigate the convergence rate picture in more details, we observe that for every 6–8 iterations the CG method using the $\boldsymbol{E}$ and $\boldsymbol{H}$ formulation and the $\boldsymbol{W}^{\mathrm{E}}$ and $\boldsymbol{W}^{\mathrm{H}}$ formulation do not yield a substantial improvement. This is caused by the fact that for the present full wave

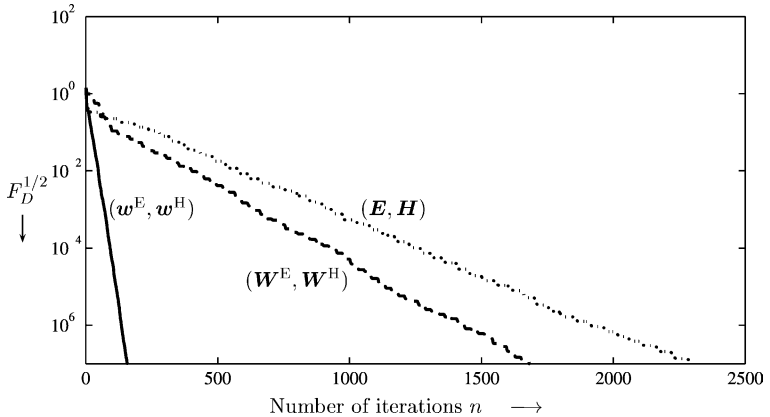

Fig. 2. The square root of the normalized error F_D with respect to the configuration given in Fig. 1 using $(\boldsymbol{E},\boldsymbol{H})$-formulation (dashed-dot line), $(\boldsymbol{W}^{\mathrm{E}},\boldsymbol{W}^{\mathrm{H}})$-formulation (dashed line) and $(\boldsymbol{w}^{\mathrm{E}},\boldsymbol{w}^{\mathrm{H}})$-formulation (solid line).

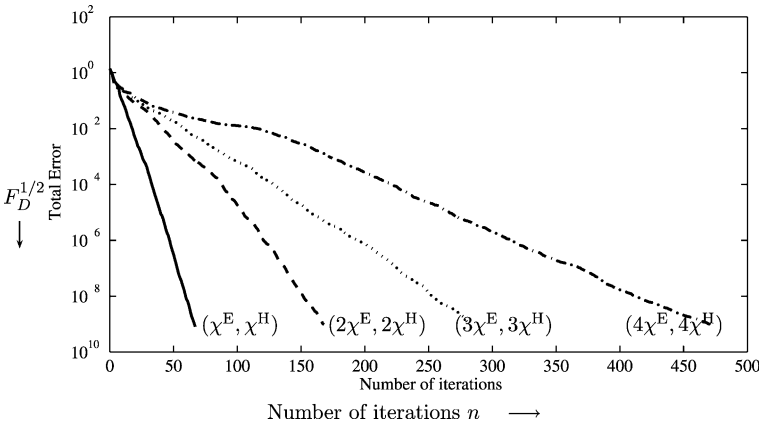

Fig. 3. The square root of the normalized error F_D with respect to the configuration given in Fig. 1 using $(\boldsymbol{w}^E, \boldsymbol{w}^H)$-formulation for increasing contrast values.

problem the values of the electric type fields and the magnetic type fields can significantly differ. Hence, normalization using the characteristic impedance Z_b is a prerequisite to obtain the solution within a reasonable number of iterations. This normalization should be of importance in the inverse problem as well.

Next in order to investigate the behavior of our forward scheme with respect to the increasing contrast values, we present in Fig. 3 the convergence rate of the scheme using $(\boldsymbol{w}^E, \boldsymbol{w}^H)$-formulation versus the number of iteration for increasing contrast values, (χ^E, χ^H), $(2\chi^E, 2\chi^H)$, $(3\chi^E, 3\chi^H)$ and $(4\chi^E, 4\chi^H)$. As we expected the convergence rate is decrease with increasing values of the electric and magnetic contrasts.

In our next example, we consider an object which has both electric and magnetic contrasts shown in Fig. 4. The rectangular object O_1 with dimension of λ by λ by λ is contained in another rectangular object

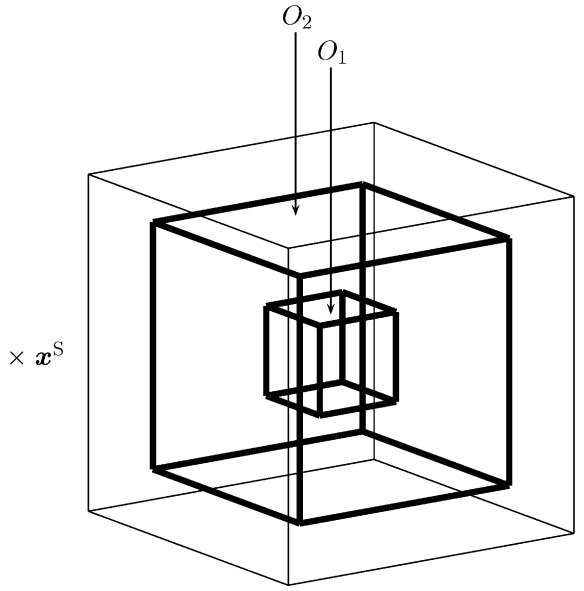

Fig. 4. A λ by λ by λ rectangular object O_1 inside a 2λ by 2λ by 2λ rectangular object O_2 in the computational domain D.

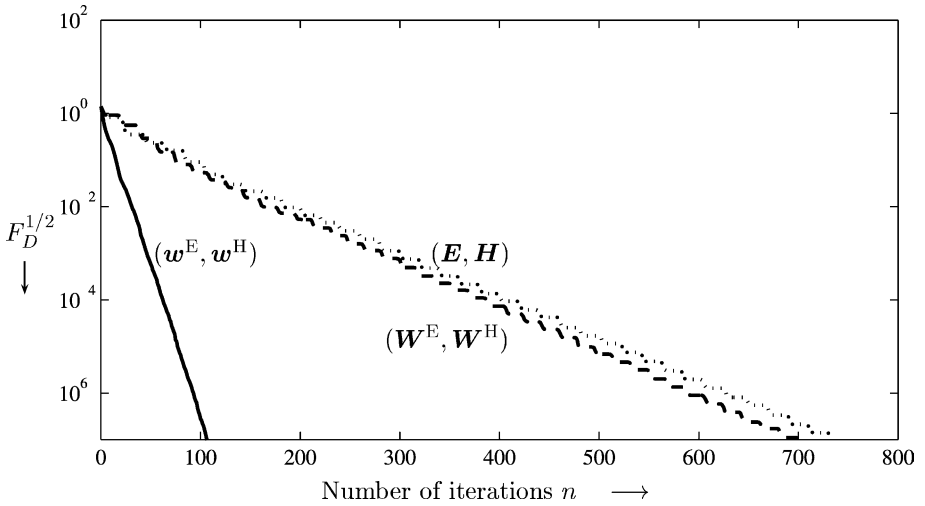

Fig. 5. The square root of the normalized error F_D with respect to the configuration given in Fig. 4 using $(\boldsymbol{E}, \boldsymbol{H})$-formulation (dashed-dot line), $(\boldsymbol{W}^{\mathrm{E}}, \boldsymbol{W}^{\mathrm{H}})$-formulation (dashed line) and $(\boldsymbol{w}^{\mathrm{E}}, \boldsymbol{w}^{\mathrm{H}})$-formulation (solid line).

with dimension of 2λ by 2λ by 2λ. The contrasts of O_1 are $\chi^{\mathrm{E}} = 0.6 + \mathrm{i}0.2$ and $\chi^{\mathrm{H}} = 0.4$, while the contrasts of O_2 are $\chi^{\mathrm{E}} = 0.3 + \mathrm{i}0.4$ and $\chi^{\mathrm{H}} = 0.2$. The background is vacuum ($\sigma_{\mathrm{b}} = 0$, $\varepsilon_{\mathrm{b}} = \varepsilon_0$ and $\mu_{\mathrm{b}} = \mu_0$). The same discretization points are used as in the previous example.

In Fig. 5 we present the convergence rate picture (the square root of the cost functional of (23) plotted against the number of iterations) of the CG method using field formulations $\boldsymbol{E}$ and $\boldsymbol{H}$ (see dashed-dotted line), using contrast sources formulations $\boldsymbol{W}^{\mathrm{E}}$ and $\boldsymbol{W}^{\mathrm{H}}$ (see dashed line) and using normalized contrast sources formulations $\boldsymbol{w}^{\mathrm{E}}$ and $\boldsymbol{w}^{\mathrm{H}}$ (see solid line). Again, we observe the necessity of using the integral equation formulated in terms of $\boldsymbol{w}^{\mathrm{E}}$ and $\boldsymbol{w}^{\mathrm{H}}$ given in (8) and (9). Advocated by these two representative numerical examples, for our inverse problems, we proceed by using the domain integral equation formulated in terms of $\boldsymbol{w}^{\mathrm{E}}$ and $\boldsymbol{w}^{\mathrm{H}}$.

4. Inverse scattering problem

We now assume that the inhomogeneous domain D is irradiated successively by a number ($j = 1, 2, \ldots$) of incident fields. For each excitation, the forward scattering problem may be reformulated as the domain integral equation, see (20) where the operators $\mathscr{L}_D^{\mathrm{EE,EH,HE,HH}}$ depend on the electric and magnetic contrasts which are also unknown. To show these unknowns explicitly we rewrite (20) as

$$\begin{bmatrix} \chi^{\mathrm{E}} \boldsymbol{E}_j^{\mathrm{inc}} \\ \chi^{\mathrm{H}} Z_{\mathrm{b}} \boldsymbol{H}_j^{\mathrm{inc}} \end{bmatrix} = \begin{bmatrix} \boldsymbol{w}_j^{\mathrm{E}} \\ \boldsymbol{w}_j^{\mathrm{H}} \end{bmatrix} - \begin{bmatrix} \chi^{\mathrm{E}} & 0 \\ 0 & \chi^{\mathrm{H}} \end{bmatrix} \begin{bmatrix} \mathscr{K}_D^{\mathrm{EE}} & \mathscr{K}_D^{\mathrm{EH}} \\ \mathscr{K}_D^{\mathrm{HE}} & \mathscr{K}_D^{\mathrm{HH}} \end{bmatrix} \begin{bmatrix} \boldsymbol{w}_j^{\mathrm{E}} \\ \boldsymbol{w}_j^{\mathrm{H}} \end{bmatrix} \quad \text{on } D, \tag{35}$$

where

$$(\mathscr{K}_D^{\mathrm{EE}} \boldsymbol{w}_j^{\mathrm{E}} + \mathscr{K}_D^{\mathrm{EH}} \boldsymbol{w}_j^{\mathrm{H}})_{\kappa;m,n,p,j} = (k_{\mathrm{b}}^2 A^{\mathrm{E}}_{\kappa;m,n,p,j} + B^{\mathrm{E}}_{\kappa;m,n,p,j}), \tag{36}$$

$$(\mathscr{K}_D^{\mathrm{HE}} \boldsymbol{w}_j^{\mathrm{E}} + \mathscr{K}_D^{\mathrm{HH}} \boldsymbol{w}_j^{\mathrm{H}})_{\kappa;m,n,p,j} = (k_{\mathrm{b}}^2 A^{\mathrm{H}}_{\kappa;m,n,p,j} + B^{\mathrm{H}}_{\kappa;m,n,p,j}) \tag{37}$$

for $\kappa = 1, 2, 3$, $m = 1, \ldots, M$, $n = 1, \ldots, N$, $p = 1, \ldots, P$, and in which $B^{\mathrm{E}}_{\kappa;m,n,p,j}$, $B^{\mathrm{H}}_{\kappa;m,n,p,j}$, $A^{\mathrm{E}}_{\kappa;m,n,p,j}$ and $A^{\mathrm{H}}_{\kappa;m,n,p,j}$ follow from (A.10)–(A.12) by adding the subscript j to denote the excitation dependency. Eq. (35) is referred as the object equation that holds in the object domain D.

Further, in the inverse problem, we measure all the components of the scattered electric field vector $\boldsymbol{E}^{\mathrm{sct}}_j$ and the scattered magnetic field vector $\boldsymbol{H}^{\mathrm{sct}}_j$ at the measurement points $\boldsymbol{x}^{\mathrm{R}}$. We assume that all measurement points are located in the data domain S, outside the object domain D. These measurement fields can also be written in the operator-matrix notation as follows:

$$\begin{bmatrix} \boldsymbol{E}^{\mathrm{sct}}_j \\ Z_{\mathrm{b}}\boldsymbol{H}^{\mathrm{sct}}_j \end{bmatrix} = \begin{bmatrix} \mathscr{K}^{\mathrm{EE}}_S & \mathscr{K}^{\mathrm{EH}}_S \\ \mathscr{K}^{\mathrm{HE}}_S & \mathscr{K}^{\mathrm{HH}}_S \end{bmatrix} \begin{bmatrix} \boldsymbol{w}^{\mathrm{E}}_j \\ \boldsymbol{w}^{\mathrm{H}}_j \end{bmatrix} \quad \text{on } S, \tag{38}$$

where

$$\left[\mathscr{K}^{\mathrm{EE}}_S \boldsymbol{w}^{\mathrm{E}}_j + \mathscr{K}^{\mathrm{EH}}_S \boldsymbol{w}^{\mathrm{H}}_j\right]_\kappa (\boldsymbol{x}^{\mathrm{R}}) = k^2_{\mathrm{b}} A^{\mathrm{E}}_{\kappa;j}(\boldsymbol{x}^{\mathrm{R}}) + B^{\mathrm{E}}_{\kappa;j}(\boldsymbol{x}^{\mathrm{R}}), \tag{39}$$

$$\left[\mathscr{K}^{\mathrm{HE}}_S \boldsymbol{w}^{\mathrm{E}}_j + \mathscr{K}^{\mathrm{HH}}_S \boldsymbol{w}^{\mathrm{H}}_j\right]_\kappa (\boldsymbol{x}^{\mathrm{R}}) = k^2_{\mathrm{b}} A^{\mathrm{H}}_{\kappa;j}(\boldsymbol{x}^{\mathrm{R}}) + B^{\mathrm{H}}_{\kappa;j}(\boldsymbol{x}^{\mathrm{R}}) \tag{40}$$

for $\boldsymbol{x}^{\mathrm{R}} \in S$ and in which $B^{\mathrm{E}}_{\kappa;j}(\boldsymbol{x}^{\mathrm{R}})$, $B^{\mathrm{H}}_{\kappa;j}(\boldsymbol{x}^{\mathrm{R}})$, $A^{\mathrm{E}}_{\kappa;j}(\boldsymbol{x}^{\mathrm{R}})$ and $A^{\mathrm{E}}_{\kappa;j}(\boldsymbol{x}^{\mathrm{R}})$ follow from (C.3)–(C.5) by adding the subscript j to denote the excitation dependency. Eq. (38) is referred as the data equation that holds in the data domain S.

The inverse scattering problems can be formulated as follows: solving the data equation in (38) to determine the electric contrast χ^{E} and magnetic contrast χ^{H} on the object domain D from the knowledge of the incident fields $\boldsymbol{E}^{\mathrm{inc}}_j$ and $\boldsymbol{H}^{\mathrm{inc}}_j$ on the object domain D and the scattered fields $\boldsymbol{E}^{\mathrm{sct}}_j$ and $\boldsymbol{H}^{\mathrm{sct}}_j$ on the data domain S subject to additional and necessary conditions that the contrast sources $\boldsymbol{w}^{\mathrm{E}}_j$ and $\boldsymbol{w}^{\mathrm{H}}_j$ and the contrasts χ^{E} and χ^{H} satisfy the object equation in (35). This is a nonlinear problem and in practice it can only be solved iteratively due to a large number of unknowns especially for the case discuss in this paper. The inverse problem at hand will be solved with the Contrast Source Inversion (CSI) method using multiplicative regularization factor.

4.1. Contrast Source Inversion method

The CSI method, developed by van den Berg and Kleinman [29] for the case of two-dimensional electromagnetic TM polarization, was extended to the full three-dimensional case for geophysical and medical applications by Abubakar and co-authors [2–5,7]. All the above-mentioned publications focus on the problem with electric contrast only. Here, we extend it to the case of handling both electric and magnetic contrast. We start with the non-regularized CSI method. In this method, the sequences of $\boldsymbol{w}^{\mathrm{E}}_{j,n}$, $\boldsymbol{w}^{\mathrm{H}}_{j,n}$, χ^{E}_n and χ^{H}_n, for $n = 1, 2, \ldots$, are iteratively found by minimizing a cost functional. The cost functional is defined as the superposition of the normalized data and object errors

$$F_n(\boldsymbol{w}^{\mathrm{E}}_j, \boldsymbol{w}^{\mathrm{H}}_j, \chi^{\mathrm{E}}, \chi^{\mathrm{H}}) = F^{\mathrm{E}}_S(\boldsymbol{w}^{\mathrm{E}}_j, \boldsymbol{w}^{\mathrm{H}}_j) + F^{\mathrm{E}}_{D,n}(\boldsymbol{w}^{\mathrm{E}}_j, \boldsymbol{w}^{\mathrm{H}}_j, \chi^{\mathrm{E}}) + F^{\mathrm{H}}_S(\boldsymbol{w}^{\mathrm{E}}_j, \boldsymbol{w}^{\mathrm{H}}_j) + F^{\mathrm{H}}_{D,n}(\boldsymbol{w}^{\mathrm{E}}_j, \boldsymbol{w}^{\mathrm{H}}_j, \chi^{\mathrm{H}}), \tag{41}$$

where the normalized data errors F^{E}_S and F^{H}_S are given by

$$F^{\mathrm{E}}_S(\boldsymbol{w}^{\mathrm{E}}_j, \boldsymbol{w}^{\mathrm{H}}_j) = \eta^{\mathrm{E}}_S \sum_j \|\boldsymbol{E}^{\mathrm{sct}}_j - \mathscr{K}^{\mathrm{EE}}_S \boldsymbol{w}^{\mathrm{E}}_j - \mathscr{K}^{\mathrm{EH}}_S \boldsymbol{w}^{\mathrm{H}}_j\|^2_S, \tag{42}$$

$$F^{\mathrm{H}}_S(\boldsymbol{w}^{\mathrm{E}}_j, \boldsymbol{w}^{\mathrm{H}}_j) = \eta^{\mathrm{H}}_S \sum_j \|Z_{\mathrm{b}}\boldsymbol{H}^{\mathrm{sct}}_j - \mathscr{K}^{\mathrm{HE}}_S \boldsymbol{w}^{\mathrm{E}}_j - \mathscr{K}^{\mathrm{HH}}_S \boldsymbol{w}^{\mathrm{H}}_j\|^2_S, \tag{43}$$

and the normalized object errors $F^{\mathrm{E}}_{D,n}$ and $F^{\mathrm{H}}_{D,n}$ by

$$F^{\mathrm{E}}_{D,n}(\boldsymbol{w}^{\mathrm{E}}_j,\boldsymbol{w}^{\mathrm{H}}_j,\chi^{\mathrm{E}}) = \eta^{\mathrm{E}}_{D,n}\sum_j \|\chi^{\mathrm{E}}\boldsymbol{E}^{\mathrm{inc}}_j - \boldsymbol{w}^{\mathrm{E}}_j + \chi^{\mathrm{E}}\mathscr{K}^{\mathrm{EE}}_D\boldsymbol{w}^{\mathrm{E}}_j + \chi^{\mathrm{E}}\mathscr{K}^{\mathrm{EH}}_D\boldsymbol{w}^{\mathrm{H}}_j\|^2_D, \tag{44}$$

$$F^{\mathrm{H}}_{D,n}(\boldsymbol{w}^{\mathrm{E}}_j,\boldsymbol{w}^{\mathrm{H}}_j,\chi^{\mathrm{H}}) = \eta^{\mathrm{H}}_{D,n}\sum_j \|\chi^{\mathrm{H}}Z_{\mathrm{b}}\boldsymbol{H}^{\mathrm{inc}}_j - \boldsymbol{w}^{\mathrm{H}}_j + \chi^{\mathrm{H}}\mathscr{K}^{\mathrm{HE}}_D\boldsymbol{w}^{\mathrm{E}}_j + \chi^{\mathrm{H}}\mathscr{K}^{\mathrm{HH}}_D\boldsymbol{w}^{\mathrm{H}}_j\|^2_D, \tag{45}$$

in which the various normalization factors are chosen to be

$$\eta^{\mathrm{E}}_S = \sum_j \|\boldsymbol{E}^{\mathrm{sct}}_j\|^2_S \quad \text{and} \quad \eta^{\mathrm{E}}_{D,n} = \sum_j \|\chi^{\mathrm{E}}_{n-1}\boldsymbol{E}^{\mathrm{inc}}_j\|^2_D, \tag{46}$$

$$\eta^{\mathrm{H}}_S = \sum_j \|Z_{\mathrm{b}}\boldsymbol{H}^{\mathrm{sct}}_j\|^2_S \quad \text{and} \quad \eta^{\mathrm{H}}_{D,n} = \sum_j \|\chi^{\mathrm{H}}_{n-1}Z_{\mathrm{b}}\boldsymbol{H}^{\mathrm{inc}}_j\|^2_D. \tag{47}$$

Here the norm $\|\cdot\|^2_D$ denotes the squared norm on object domain D defined in (21), and while the norm $\|\cdot\|^2_S$ on the data domain S is defined as

$$\|\boldsymbol{u}\|^2_S = \sum_{\forall \boldsymbol{x}\in S} \boldsymbol{u}(\boldsymbol{x})\cdot\overline{\boldsymbol{u}(\boldsymbol{x})}. \tag{48}$$

The normalization factors in (46) and (47) are chosen in such a way that all the terms in (41) are equal to unity if the contrast sources $\boldsymbol{w}^{\mathrm{E}}_j$ and $\boldsymbol{w}^{\mathrm{H}}_j$ vanish. Although this updating of the contrast sources and contrasts can be carried out simultaneously, an alternating updating scheme simplifies the algorithm significantly. In addition it is noted that, for given contrasts χ^{E} and χ^{H}, the second and the fourth terms in (41) make the problem to determine the contrast sources well-posed. Hence, these terms F^{E}_D and F^{H}_D can also be seen as physical regularizer (Maxwell's regularizers) terms for the data errors F^{E}_S and F^{H}_S and the choice to update the unknown contrast sources and contrasts alternatingly seems to be a natural choice.

4.1.1. Updating the contrast sources

For given $\boldsymbol{w}^{\mathrm{E}}_{j,n-1}$, $\boldsymbol{w}^{\mathrm{H}}_{j,n-1}$, χ^{E}_{n-1} and χ^{H}_{n-1}, in each iteration, we update the contrast sources using a single CG step as

$$\begin{bmatrix}\boldsymbol{w}^{\mathrm{E}}_{j,n}\\ \boldsymbol{w}^{\mathrm{H}}_{j,n}\end{bmatrix} = \begin{bmatrix}\boldsymbol{w}^{\mathrm{E}}_{j,n-1}\\ \boldsymbol{w}^{\mathrm{H}}_{j,n-1}\end{bmatrix} + \alpha_n\begin{bmatrix}\boldsymbol{v}^{\mathrm{E}}_{j,n}\\ \boldsymbol{v}^{\mathrm{H}}_{j,n}\end{bmatrix}, \tag{49}$$

where α_n is a real parameter independent of position, while $\boldsymbol{v}^{\mathrm{E}}_{j,n}$ and $\boldsymbol{v}^{\mathrm{H}}_{j,n}$ are the Polak–Ribière conjugate gradient directions given by

$$\begin{bmatrix}\boldsymbol{v}^{\mathrm{E}}_{j,0}\\ \boldsymbol{v}^{\mathrm{H}}_{j,0}\end{bmatrix} = \begin{bmatrix}\boldsymbol{0}\\ \boldsymbol{0}\end{bmatrix}, \quad \begin{bmatrix}\boldsymbol{v}^{\mathrm{E}}_{j,n}\\ \boldsymbol{v}^{\mathrm{H}}_{j,n}\end{bmatrix} = \begin{bmatrix}\boldsymbol{g}^{\mathrm{E}}_{j,n}\\ \boldsymbol{g}^{\mathrm{H}}_{j,n}\end{bmatrix} + \gamma_n\begin{bmatrix}\boldsymbol{v}^{\mathrm{E}}_{j,n-1}\\ \boldsymbol{v}^{\mathrm{H}}_{j,n-1}\end{bmatrix}, \tag{50}$$

in which

$$\gamma_n = \frac{\sum_j \mathrm{Re}\langle \boldsymbol{g}^{\mathrm{E}}_{j,n}, \boldsymbol{g}^{\mathrm{E}}_{j,n} - \boldsymbol{g}^{\mathrm{E}}_{j,n-1}\rangle_D + \sum_j \mathrm{Re}\langle \boldsymbol{g}^{\mathrm{H}}_{j,n}, \boldsymbol{g}^{\mathrm{H}}_{j,n} - \boldsymbol{g}^{\mathrm{H}}_{j,n-1}\rangle_D}{\sum_j \|\boldsymbol{g}^{\mathrm{E}}_{j,n-1}\|^2_D + \sum_j \|\boldsymbol{g}^{\mathrm{H}}_{j,n-1}\|^2_D}. \tag{51}$$

In (50) and (51), the gradients $\boldsymbol{g}^{\mathrm{E}}_{j,n}$ and $\boldsymbol{g}^{\mathrm{H}}_{j,n}$ of the cost functional F_n in (41) with respect to $\boldsymbol{w}^{\mathrm{E}}_j$ and $\boldsymbol{w}^{\mathrm{H}}_j$ evaluated at $\boldsymbol{w}^{\mathrm{E}}_{j,n-1}$, $\boldsymbol{w}^{\mathrm{H}}_{j,n-1}$, χ^{H}_{n-1} and χ^{E}_{n-1} are given by

$$\begin{bmatrix} \boldsymbol{g}^{\mathrm{E}}_{j,n} \\ \boldsymbol{g}^{\mathrm{H}}_{j,n} \end{bmatrix} = \begin{bmatrix} \eta^{\mathrm{E}}_S \mathscr{K}^{\mathrm{EE}*}_S & \eta^{\mathrm{H}}_S \mathscr{K}^{\mathrm{HE}*}_S \\ \eta^{\mathrm{E}}_S \mathscr{K}^{\mathrm{EH}*}_S & \eta^{\mathrm{H}}_S \mathscr{K}^{\mathrm{HH}*}_S \end{bmatrix} \begin{bmatrix} \boldsymbol{\rho}^{\mathrm{E}}_{j,n-1} \\ \boldsymbol{\rho}^{\mathrm{H}}_{j,n-1} \end{bmatrix} + \begin{bmatrix} \eta^{\mathrm{E}}_{D,n}(\mathscr{I} - \mathscr{K}^{\mathrm{EE}*}_D) & \eta^{\mathrm{H}}_{D,n} \mathscr{K}^{\mathrm{HE}*}_D \\ \eta^{\mathrm{E}}_{D,n} \mathscr{K}^{\mathrm{EH}*}_D & \eta^{\mathrm{H}}_{D,n}(\mathscr{I} - \mathscr{K}^{\mathrm{HH}*}_D) \end{bmatrix} \begin{bmatrix} \boldsymbol{r}^{\mathrm{E}}_{j,n-1} \\ \boldsymbol{r}^{\mathrm{H}}_{j,n-1} \end{bmatrix}, \tag{52}$$

where $\mathscr{K}^{\mathrm{EE}*}_S$, $\mathscr{K}^{\mathrm{EH}*}_S$, $\mathscr{K}^{\mathrm{HE}*}_S$, $\mathscr{K}^{\mathrm{HH}*}_S$, $\mathscr{K}^{\mathrm{EE}*}_D$, $\mathscr{K}^{\mathrm{EH}*}_D$, $\mathscr{K}^{\mathrm{HE}*}_D$ and $\mathscr{K}^{\mathrm{HH}*}_D$ are the adjoint operators of $\mathscr{K}^{\mathrm{EE}}_S$, $\mathscr{K}^{\mathrm{EH}}_S$, $\mathscr{K}^{\mathrm{HE}}_S$, $\mathscr{K}^{\mathrm{HH}}_S$, $\mathscr{K}^{\mathrm{EE}}_D$, $\mathscr{K}^{\mathrm{EH}}_D$, $\mathscr{K}^{\mathrm{HE}}_D$ and $\mathscr{K}^{\mathrm{HH}}_D$, respectively. The discretized versions of these adjoint operators can be found in Appendices B and C. Further, the residuals in the data and object domain are defined as

$$\boldsymbol{\rho}^{\mathrm{E}}_{j,n} = \boldsymbol{E}^{\mathrm{sct}}_j - \mathscr{K}^{\mathrm{EE}}_S \boldsymbol{w}^{\mathrm{E}}_{j,n} - \mathscr{K}^{\mathrm{EH}}_S \boldsymbol{w}^{\mathrm{H}}_{j,n}, \tag{53}$$

$$\boldsymbol{\rho}^{\mathrm{H}}_{j,n} = Z_{\mathrm{b}} \boldsymbol{H}^{\mathrm{sct}}_j - \mathscr{K}^{\mathrm{HE}}_S \boldsymbol{w}^{\mathrm{E}}_{j,n} - \mathscr{K}^{\mathrm{HH}}_S \boldsymbol{w}^{\mathrm{H}}_{j,n} \tag{54}$$

and

$$\boldsymbol{r}^{\mathrm{E}}_{j,n} = \chi^{\mathrm{E}}_{n-1} \boldsymbol{E}^{\mathrm{inc}}_j - \boldsymbol{w}^{\mathrm{E}}_{j,n} + \chi^{\mathrm{E}}_{n-1} \mathscr{K}^{\mathrm{EE}}_D \boldsymbol{w}^{\mathrm{E}}_{j,n} + \chi^{\mathrm{E}}_{n-1} \mathscr{K}^{\mathrm{EH}}_D \boldsymbol{w}^{\mathrm{H}}_{j,n}, \tag{55}$$

$$\boldsymbol{r}^{\mathrm{H}}_{j,n} = \chi^{\mathrm{H}}_{n-1} Z_{\mathrm{b}} \boldsymbol{H}^{\mathrm{inc}}_j - \boldsymbol{w}^{\mathrm{H}}_{j,n} + \chi^{\mathrm{H}}_{n-1} \mathscr{K}^{\mathrm{HE}}_D \boldsymbol{w}^{\mathrm{E}}_{j,n} + \chi^{\mathrm{H}}_{n-1} \mathscr{K}^{\mathrm{HH}}_D \boldsymbol{w}^{\mathrm{H}}_{j,n}, \tag{56}$$

respectively. The real parameter α_n is found as the minimizer of

$$\alpha_n = \arg \min_{\text{real } \alpha} \left\{ \mathrm{F_n}(\boldsymbol{w}^{\mathrm{E}}_{\mathrm{j,n-1}} + \alpha \boldsymbol{v}^{\mathrm{E}}_{\mathrm{j,n}}, \boldsymbol{w}^{\mathrm{H}}_{\mathrm{j,n-1}} + \alpha \boldsymbol{v}^{\mathrm{H}}_{\mathrm{j,n}}, \chi^{\mathrm{E}}_{\mathrm{n-1}}, \chi^{\mathrm{H}}_{\mathrm{n-1}}) \right\}. \tag{57}$$

Note that the cost functional F_n is a quadratic function of real α, hence only one minimizer is arrived at. Substituting (49) in (57) and then minimizing (41), we obtain an explicit expression for the minimizer.

4.1.2. Updating the contrasts

Before we proceed with updating the contrasts χ^{E} and χ^{H}, we observe that the unknown electric contrast only occurs in the normalized object error $F^{\mathrm{E}}_{D,n}$, while the unknown magnetic contrast only occurs in the normalized object error $F^{\mathrm{H}}_{D,n}$. Hence, for given contrast sources $\boldsymbol{w}^{\mathrm{E}}_j$ and $\boldsymbol{w}^{\mathrm{H}}_j$, the minimization problem is uncoupled. In order to find these contrasts, we need only to minimize the normalized object errors defined in (44) and (45) separately. We rewrite these two cost functional as

$$F^{\mathrm{E}}_{D,n}(\boldsymbol{w}^{\mathrm{E}}_{j,n}, \boldsymbol{w}^{\mathrm{H}}_{j,n}, \chi^{\mathrm{E}}) = \eta^{\mathrm{E}}_{D,n} \sum_j \| \chi^{\mathrm{E}} \boldsymbol{f}^{\mathrm{E}}_{j,n} - \boldsymbol{w}^{\mathrm{E}}_{j,n} \|^2_D, \tag{58}$$

$$F^{\mathrm{H}}_{D,n}(\boldsymbol{w}^{\mathrm{E}}_{j,n}, \boldsymbol{w}^{\mathrm{H}}_{j,n}, \chi^{\mathrm{H}}) = \eta^{\mathrm{H}}_{D,n} \sum_j \| \chi^{\mathrm{H}} \boldsymbol{f}^{\mathrm{H}}_{j,n} - \boldsymbol{w}^{\mathrm{H}}_{j,n} \|^2_D, \tag{59}$$

where, for given contrast sources $\boldsymbol{w}^{\mathrm{E}}_{j,n}$ and $\boldsymbol{w}^{\mathrm{H}}_{j,n}$,

$$\boldsymbol{f}^{\mathrm{E}}_{j,n} = \boldsymbol{E}^{\mathrm{inc}}_j + \mathscr{K}^{\mathrm{EE}}_D \boldsymbol{w}^{\mathrm{E}}_{j,n} + \mathscr{K}^{\mathrm{EH}}_D \boldsymbol{w}^{\mathrm{H}}_{j,n}, \tag{60}$$

$$\boldsymbol{f}^{\mathrm{H}}_{j,n} = Z_{\mathrm{b}} \boldsymbol{H}^{\mathrm{inc}}_j + \mathscr{K}^{\mathrm{HE}}_D \boldsymbol{w}^{\mathrm{E}}_{j,n} + \mathscr{K}^{\mathrm{HH}}_D \boldsymbol{w}^{\mathrm{H}}_{j,n}. \tag{61}$$

The minimizers χ^{E}_n and χ^{H}_n that minimize (58) and (59), respectively, are found explicitly as

$$\chi^{\mathrm{E}}_n = \frac{\sum_j \boldsymbol{w}^{\mathrm{E}}_{j,n} \cdot \overline{\boldsymbol{f}^{\mathrm{E}}_{j,n}}}{\sum_j |\boldsymbol{f}^{\mathrm{E}}_{j,n}|^2} \quad \text{and} \quad \chi^{\mathrm{H}}_n = \frac{\sum_j \boldsymbol{w}^{\mathrm{H}}_{j,n} \cdot \overline{\boldsymbol{f}^{\mathrm{H}}_{j,n}}}{\sum_j |\boldsymbol{f}^{\mathrm{H}}_{j,n}|^2}. \tag{62}$$

In view of this analytical minimization, it is anticipated that here the ill-posedness of the inverse problem has been avoided, while in other inversion methods (see e.g. [10,13,18,19]) where an integral operator acts on the contrast a numerical inversion of the ill-posed integral operator may lead to numerical instabilities.

4.1.3. Multiplicative regularization

When the number of data is limited and a significant noise level is present in the data we use the concept of multiplicative regularization [31], where the strength of regularization is determined by the error norms pertaining to the data equations and the object equations. In each iteration, the regularization factor is the norm of the relative spatial variation of the contrast. Although it is an L_2-norm it restores the band limitation of the images we have obtained with the Contrast Source Inversion method, see also [30]. In this paper we apply the multiplicative regularization technique by extending the theory developed by Abubakar et al. [9] to the more complicated case with two types of material contrasts. Since in the cost functional of (41) the unknown χ^{E} is only present in $F^{\mathrm{E}}_{D,n}$ and while the unknown χ^{H} only in $F^{\mathrm{H}}_{D,n}$, we multiply the normalized errors corresponding to the electric type integral with the regularization factor for χ^{E} only and to the magnetic type integral with the regularization factor for χ^{H} only. Then, in the inversion process we aim to minimize the norms

$$\mathscr{F}^{\mathrm{E}}_n(\boldsymbol{w}^{\mathrm{E}}_j, \boldsymbol{w}^{\mathrm{H}}_j, \chi^{\mathrm{E}}) = \Big[F^{\mathrm{E}}_S(\boldsymbol{w}^{\mathrm{E}}_j, \boldsymbol{w}^{\mathrm{H}}_j) + F^{\mathrm{E}}_{D,n}(\boldsymbol{w}^{\mathrm{E}}_j, \boldsymbol{w}^{\mathrm{H}}_j, \chi^{\mathrm{E}})\Big] F^{\mathrm{R}}_n(\nabla\chi^{\mathrm{E}}), \tag{63}$$

$$\mathscr{F}^{\mathrm{H}}_n(\boldsymbol{w}^{\mathrm{E}}_j, \boldsymbol{w}^{\mathrm{H}}_j, \chi^{\mathrm{H}}) = \Big[F^{\mathrm{H}}_S(\boldsymbol{w}^{\mathrm{E}}_j, \boldsymbol{w}^{\mathrm{H}}_j) + F^{\mathrm{H}}_{D,n}(\boldsymbol{w}^{\mathrm{E}}_j, \boldsymbol{w}^{\mathrm{H}}_j, \chi^{\mathrm{H}})\Big] F^{\mathrm{R}}_n(\nabla\chi^{\mathrm{H}}), \tag{64}$$

separately, where $\nabla\chi^{\mathrm{E}}$ and $\nabla\chi^{\mathrm{H}}$ denote the gradient of the electric and magnetic contrasts, respectively. The non-zero regularization factors F^{R}_n in (63) and (64) are weighted L^2-norm factors, viz.,

$$F^{R}_n(\nabla\chi^{\mathrm{E}}) = \frac{1}{V}\int_D \frac{|\nabla\chi^{\mathrm{E}}(\boldsymbol{x})|^2 + (\delta^{\mathrm{E}}_n)^2}{|\nabla\chi^{\mathrm{E}}_{n-1}(\boldsymbol{x})|^2 + (\delta^{\mathrm{E}}_n)^2}\,\mathrm{d}v(\boldsymbol{x}) = \|b^{\mathrm{E}}_n\nabla\chi^{\mathrm{E}}\|^2_D + (\delta^{\mathrm{E}}_n)^2\|b^{\mathrm{E}}_n\|^2_D, \tag{65}$$

where

$$b^{\mathrm{E}}_n = \frac{1}{V^{1/2}\Big[\big|\nabla\chi^{\mathrm{E}}_{n-1}(\boldsymbol{x})\big|^2 + (\delta^{\mathrm{E}}_n)^2\Big]^{1/2}}, \quad \text{with} \quad V = \int_D \mathrm{d}v(\boldsymbol{x}), \tag{66}$$

and $F^{R}_n(\nabla\chi^{\mathrm{H}})$ follows from (65) and (66) by replacing χ^{E}, δ^{E}_n and b^{E}_n with χ^{H}, δ^{H}_n and b^{H}_n. From this point on we will discuss only the updating procedure for χ^{E}, while the updating procedure for χ^{H} follows from replacing the superscript $^{\mathrm{E}}$ in the updating formulas for χ^{E} by the superscript $^{\mathrm{H}}$.

Whether the multiplicative functional of the form of (65) provides a regularized solution of the inverse problem in the general case is still an open problem, but we now discuss some measures to obtain regularized solutions with our CSI algorithm. The steering parameter $(\delta^{\mathrm{E}}_n)^2$ controls the influence of the regularization. However, the choice of these steering parameter is significant less sensitive to the solution than the choice of the parameter in the framework of an additive Tikhonov regularization. Similar to the so-called adaptive regularization with progressively decreasing parameter in the framework of Tikhonov regularization (see e.g. [35]) we take a progressively decreasing steering parameter. Since the normalized object error term will decrease as a function of the number of iterations, despite of the amount of the noise present in the data, it is natural to take the steering parameters as

$$(\delta^{\mathrm{E}}_n)^2 = \frac{F^{\mathrm{E}}_{D,n}(\boldsymbol{w}^{\mathrm{E}}_{j,n}, \boldsymbol{w}^{\mathrm{H}}_{j,n}, \chi^{\mathrm{E}}_{n-1})}{[\max(\Delta x_1, \Delta x_2, \Delta_3)]^2}. \tag{67}$$

The structure of our multiplicative regularization procedure is such that it will minimize the regularization factor with large weighting parameter in the beginning of the optimization process, because the value of $F_S^{\mathrm{E}} + F_{D,n}^{\mathrm{E}}$ is still large, and that it will gradually minimize more and more the error in the data and object equations when the regularization factor F_n^R remains nearly constant value. If noise is present in the data, the normalized data error will remain at large values during the optimization and, therefore, the weight of the regularization factor will be more significant. Hence, the noise will, at all times, be suppressed in the reconstruction process and we automatically fulfill the need of larger regularization when the data contains noise.

Since the regularization factor have the properties $F_n^{\mathrm{R}}(\nabla\chi_{n-1}^{\mathrm{E}}) = 1$, there is no change in the updating procedure for $\boldsymbol{w}_j^{\mathrm{E}}$ and $\boldsymbol{w}_j^{\mathrm{H}}$. At the beginning of each iteration, we have to replace the quantity χ_{n-1}^{E} and by $\chi_{n-1}^{\mathrm{R,E}}$, but the remainder of the contrast sources updating procedure are not changed. Then only the updating of the contrasts has to be modified. In fact the contrast sources are determined from a cost functional that in nature is not changed by the regularization.

Instead of taking the previous iterate of the contrast values as done in the standard CG method, we now take the analytical values of (62) as starting values. From this point, we make an additional minimization step,

$$\chi_n^{\mathrm{R,E}} = \chi_n^{\mathrm{E}} + \beta_n^{\mathrm{E}} d_n^{\mathrm{E}}, \quad d_n^{\mathrm{E}} = g_n^{\mathrm{E}} + \frac{\mathrm{Re}\langle g_n^{\mathrm{E}}, g_n^{\mathrm{E}} - g_{n-1}^{\mathrm{E}}\rangle_D}{\|g_{n-1}^{\mathrm{E}}\|_D^2} d_{n-1}^{\mathrm{E}}, \tag{68}$$

where χ_n^{E} is given in (62), β_n^{E} is a real parameter, and g_n^{E} is the gradient of the cost functional $\mathscr{F}_n^{\mathrm{E}}$ in (63) with respect to χ^{E} evaluated at $\boldsymbol{w}_{j,n}^{\mathrm{E}}$ and χ_n^{E} given by

$$g_n^{\mathrm{E}} = \left[F_S^{\mathrm{E}}(\boldsymbol{w}_{j,n}^{\mathrm{E}}, \boldsymbol{w}_{j,n}^{\mathrm{H}}) + F_{D,n}^{\mathrm{E}}(\boldsymbol{w}_{j,n}^{\mathrm{E}}, \boldsymbol{w}_{j,n}^{\mathrm{H}}, \chi_n^{\mathrm{E}})\right]\nabla \cdot \left[(b_n^{\mathrm{E}})^2 \nabla\chi^{\mathrm{E}}(\boldsymbol{x})\right]. \tag{69}$$

Note that there is no contribution from the gradient of $F_{D,n}^{\mathrm{E}}$ because around this point the corresponding gradient has vanished. Hence, we can conclude that the inclusion of this regularization factor is only an extra step which will not disturb the physical solution.

The real parameter β_n^{E} is found by minimizing the cost functional in (63) as

$$\beta_n^{\mathrm{E}} = \arg\min_{\text{real } \beta}\left[\mathrm{F}_S^{\mathrm{E}}(\boldsymbol{w}_{j,n}^{\mathrm{E}}, \boldsymbol{w}_{j,n}^{\mathrm{H}}) + \mathrm{F}_{D,n}^{\mathrm{E}}(\boldsymbol{w}_{j,n}^{\mathrm{E}}, \boldsymbol{w}_{j,n}^{\mathrm{H}}, \chi_n^{\mathrm{E}} + \beta \mathrm{d}_n^{\mathrm{E}})\right]\mathrm{F}_n^{\mathrm{R}}(\chi_n^{\mathrm{E}} + \beta \mathrm{d}_n^{\mathrm{E}}). \tag{70}$$

This minimization can be performed analytically since the cost functional $\mathscr{F}_n^{\mathrm{E}}$ is a fourth-degree polynomial in β^{E}, see [31].

A disadvantage of the multiplicative regularization with respect to the additive regularization is that we have to guarantee that the cost functional $\mathscr{F}_n^{\mathrm{E}}$ in (63) is a convex function of real β^{E}. A sufficient condition is, see [31],

$$(\delta_n^{\mathrm{E}})^2 \geqslant \frac{\|b_n^{\mathrm{E}} \nabla\chi_n^{\mathrm{E}}\|_D^2}{2\|b_n^{\mathrm{E}}\|_D^2}. \tag{71}$$

If the choice for the parameter $(\delta_n^{\mathrm{E}})^2$ of (67) is less than the right-hand side of (71), we replace the value of $(\delta_n^{\mathrm{E}})^2$ by the right-hand side of (71).

In comparison to our algorithm discussed in [31] we use now an improved preconditioner. Note that for given contrast sources $\boldsymbol{w}_j^{\mathrm{E}}$, the normal equation associated with the cost functional in (63) with respect to χ^{E} is given by

$$F_n^{\mathrm{R}}(\chi^{\mathrm{E}})\eta_{D,n}^{\mathrm{E}} \sum_j |\boldsymbol{f}_{j,n}^{\mathrm{E}}|^2 + [F_S^{\mathrm{E}}(\boldsymbol{w}_{j,n}^{\mathrm{E}}, \boldsymbol{w}_{j,n}^{\mathrm{H}}) + F_{D,n}^{\mathrm{E}}(\boldsymbol{w}_{j,n}^{\mathrm{E}}, \boldsymbol{w}_{j,n}^{\mathrm{H}}, \chi^{\mathrm{E}})]\nabla \cdot (b_n^{\mathrm{E}} \nabla\chi^{\mathrm{E}}) = \eta_{D,n}^{\mathrm{E}} \sum_j \boldsymbol{w}_{j,n}^{\mathrm{E}} \cdot \overline{\boldsymbol{f}_{j,n}^{\mathrm{E}}}. \tag{72}$$

It is clear that (72) is a nonlinear equation in terms of the electric contrast χ^{E}. We observe that the first term in (72) represents a diagonal matrix and its second term represents a very sparse matrix (for the case of one-dimensional in space it is a matrix with only three non-zero elements on its diagonal). Then, if the problem is linear, we expect that Jacobi preconditioning operator will be effective to accelerate the converge of CG type methods. The only difficulty in the present algorithm is the nonlinearity. Hence, by linearizing this normal equation (put $\chi^{\mathrm{E}} = \chi_n^{\mathrm{E}}$ in $F_{D,n}^{\mathrm{E}}$ and F_n^{R}) and taking diagonal term we can arrive at a very simple preconditioning operator for the updating procedure for the electric contrast χ^{E},

$$\mathscr{P}_n^{\mathrm{E}}\mathscr{P}_n^{\mathrm{E}*} = \mathrm{diag}^{-1}\left[\eta_{D,n}^{\mathrm{E}}\sum_j |\boldsymbol{f}_{j,n}^{\mathrm{E}}|^2 + [F_S^{\mathrm{E}}(\boldsymbol{w}_{j,n}^{\mathrm{E}}, \boldsymbol{w}_{j,n}^{\mathrm{H}}) + F_{D,n}^{\mathrm{E}}(\boldsymbol{w}_{j,n}^{\mathrm{E}}, \boldsymbol{w}_{j,n}^{\mathrm{H}}, \chi_n^{\mathrm{E}})]\nabla\cdot b_n^{\mathrm{E}}\nabla\right]. \tag{73}$$

This preconditioning operator in (73) is used in the optimization process by multiplying the gradients in (69) by $\mathscr{P}_n^{\mathrm{E}}\mathscr{P}_n^{\mathrm{E}*}$.

Finally, we note that the updating procedure for the magnetic contrast χ^{H} can be found in a similar way. After we have obtained new estimates for the contrast $\chi_n^{\mathrm{R,E}}$ and $\chi_n^{\mathrm{R,H}}$, we calculate the value of the cost functional in (41) for $\boldsymbol{w}_j^{\mathrm{E}} = \boldsymbol{w}_{j,n}^{\mathrm{E}}$, $\boldsymbol{w}_j^{\mathrm{H}} = \boldsymbol{w}_{j,n}^{\mathrm{H}}$, $\chi^{\mathrm{E}} = \chi_n^{\mathrm{R,E}}$ and $\chi^{\mathrm{H}} = \chi_n^{\mathrm{R,H}}$, and check whether it is already small enough or already reaches a minimum. If it is not, we repeat again the iterative process by updating the contrast sources starting with $\chi_{n-1}^{\mathrm{E}} = \chi_{n-1}^{\mathrm{R,E}}$ and $\chi_{n-1}^{\mathrm{H}} = \chi_{n-1}^{\mathrm{R,H}}$ of the previous iteration.

4.2. Numerical examples

In this section we present a few reconstruction results using simulated data in order to illustrate the behavior of our numerical algorithm.

4.2.1. Inversion of two disjointed electric and magnetic scatterers

As the first example, we consider the case when we have two objects, one is purely electric object with contrast $\chi^{\mathrm{E}} = 0.8 + \mathrm{i}0.4$ while the other one is a purely magnetic object with contrast $\chi^{\mathrm{H}} = 0.8$, as shown in Fig. 1. The sizes of these objects are λ by λ by λ. These unknown objects are illuminated using 63 sources located on a plane with a dimension of 3λ by 3λ with the center located at $(-1.6\lambda, 0, 0)$. These 63 vertical magnetic dipole sources are distributed uniformly on this source plane. Further we measure all components of the electric and magnetic scattered fields on a transmitter plane with the same size as the source plane, but its center is located at $(1.6\lambda, 0, 0)$. Hence we have 23,814 data points. After generation of synthetic data we added $n_{\mathrm{s}} = 10\%$ pseudo-random white noise to the data according to the following equations:

$$\widetilde{\boldsymbol{E}}_j^{\mathrm{sct}}(\boldsymbol{x}^{\mathrm{R}}) = \boldsymbol{E}_j^{\mathrm{sct}}(\boldsymbol{x}^{\mathrm{R}}) + \frac{\max\left[\forall_j \boldsymbol{E}_j^{\mathrm{sct}}(\boldsymbol{x}^{\mathrm{R}})\right]}{\sqrt{2}} n_{\mathrm{s}}(\zeta_j + \mathrm{i}\eta_j), \tag{74}$$

$$\widetilde{\boldsymbol{H}}_j^{\mathrm{sct}}(\boldsymbol{x}^{\mathrm{R}}) = \boldsymbol{H}_j^{\mathrm{sct}}(\boldsymbol{x}^{\mathrm{R}}) + \frac{\max\left[\forall_j \boldsymbol{H}_j^{\mathrm{sct}}(\boldsymbol{x}^{\mathrm{R}})\right]}{\sqrt{2}} n_{\mathrm{s}}(\zeta_j + \mathrm{i}\eta_j), \tag{75}$$

where $\widetilde{\boldsymbol{E}}_j^{\mathrm{sct}}$ and $\widetilde{\boldsymbol{H}}_j^{\mathrm{sct}}$ are the noisy data and ζ_j and η_j are random numbers with normal distribution varying from -0.5 up to 0.5.

In the inversion we assume that the unknown objects are located in the object domain D with size of 3λ by 3λ by 3λ. This domain D is divided into 30 by 30 by 30, hence in total we have 54,000 unknowns. In Figs. 6–8, we present the reconstructed results obtained with our numerical algorithm after 1024 iterations at different x_3 planes (the most top-left plot is x_3 plane at -1.45λ and the most bottom-right plot is x_3 plane at 1.45λ). In these figures the exact profile is indicated by the dashed lines. The reconstructed electric contrast

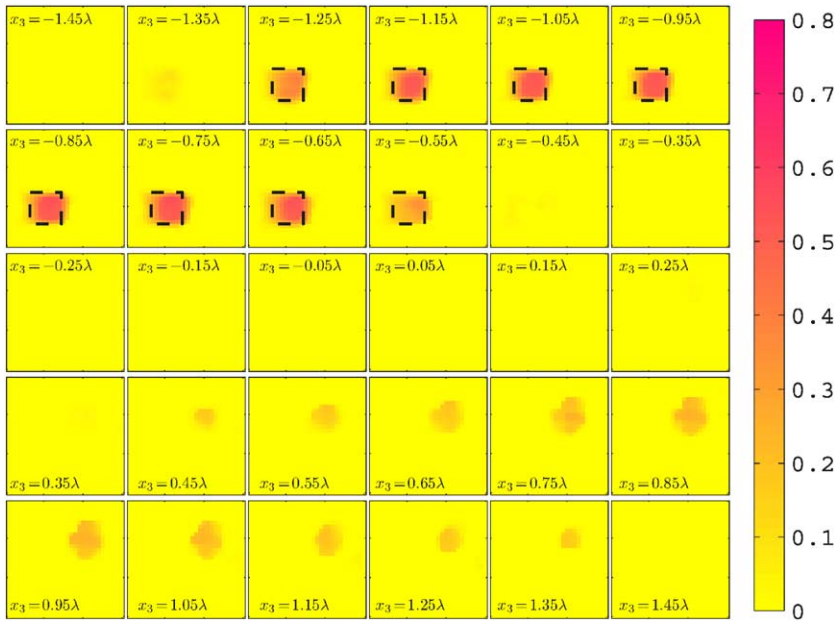

Fig. 6. Configuration of Fig. 1. The reconstructed real part of the electric contrast χ^E given in different x_3 plane. The contours of the exact profile are given by the dashed lines.

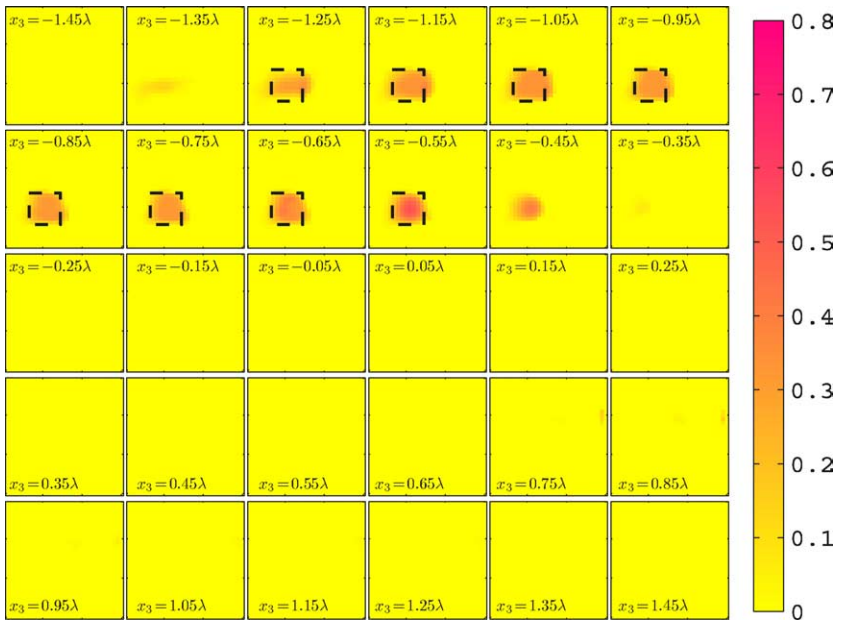

Fig. 7. Configuration of Fig. 1. The reconstructed imaginary part of the electric contrast χ^E given in different x_3 plane. The contours of the exact profile are given by the dashed lines.

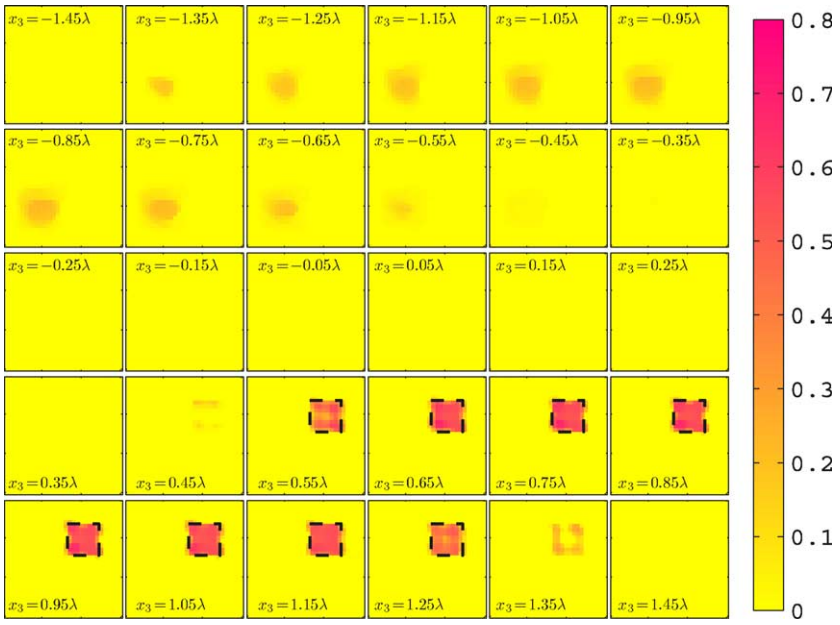

Fig. 8. Configuration of Fig. 1. The reconstructed magnetic contrast χ^{H} given in different x_3 plane. The contours of the exact profile are given by the dashed lines.

is given in Fig. 6 (its real part) and Fig. 7 (its imaginary part) while the reconstructed magnetic contrast is given in Fig. 8. After 1024 iterations the error in electric contrast and magnetic contrast are reduced to $\mathrm{ERR}^{\mathrm{E}} = 0.36$ and $\mathrm{ERR}^{\mathrm{H}} = 0.21$. The error in contrast are defined as

$$\mathrm{ERR}_n^{\mathrm{E}} = \frac{\|\chi_n^{\mathrm{E}} - \chi_{\mathrm{exact}}^{\mathrm{E}}\|_D}{\|\chi_{\mathrm{exact}}^{\mathrm{E}}\|_D} \quad \text{and} \quad \mathrm{ERR}_n^{\mathrm{H}} = \frac{\|\chi_n^{\mathrm{H}} - \chi_{\mathrm{exact}}^{\mathrm{H}}\|_D}{\|\chi_{\mathrm{exact}}^{\mathrm{H}}\|_D}. \tag{76}$$

The errors in contrast as function of iterations are given in Fig. 9.

From the results in Figs. 6–8, we can conclude that the locations and the shapes of the two rectangular objects are well reconstructed. By comparing Figs. 6 and 8, we clearly observe some cross-talk phenomena between the permittivity (the real part of the electric contrast) and the permeability (the real magnetic contrast). On the other hand, Fig. 7 indicates that there is only one lossy electric object. This positive effect might be caused by the fact that there exists no object with magnetic loss, which has been accounted for in our inversion algorithm.

Finally, one should also note that in addition to the contrast unknowns, the fields inside domain D are also unknown. The total number of the field unknowns are $6 \times 63 \times 30 \times 30 \times 30$ which is equal to the total number of known incident fields on D.

4.2.2. Inversion of scatterers with both electric and magnetic contrasts

As the next example, we consider the problem where the unknown scatterers having both electric and magnetic contrasts. The exact configuration is given in Fig. 4. The unknown cube O_1 with dimension of λ by λ by λ is contained in another cube O_2 with dimension of 2λ by 2λ by 2λ. The contrasts of cube O_1 are $\chi^{\mathrm{E}} = 0.6 + \mathrm{i}0.2$ and $\chi^{\mathrm{H}} = 0.4$, while the contrasts of cube O_2 are $\chi^{\mathrm{E}} = 0.3 + \mathrm{i}0.4$ and $\chi^{\mathrm{H}} = 0.2$. The center of these cubes are located on the origin of the Cartesian coordinate system. The background is vacuum ($\sigma_{\mathrm{b}} = 0$, $\varepsilon_{\mathrm{b}} = \varepsilon_0$ and $\mu_{\mathrm{b}} = \mu_0$). Fig. 10(a) presents the three-dimensional volume slices of the exact electric

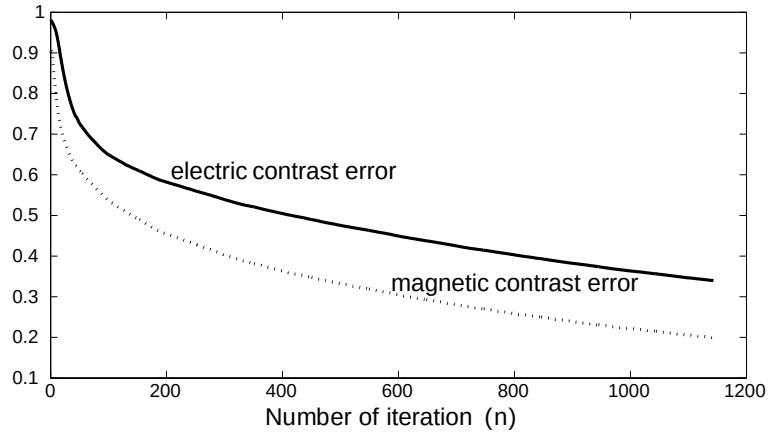

Fig. 9. The error in electric contrast $\mathrm{ERR}^{\mathrm{E}}$ (solid line) and magnetic contrast $\mathrm{ERR}^{\mathrm{H}}$ (dashed line) as function of iteration n of two disjointed electric and magnetic scatterers.

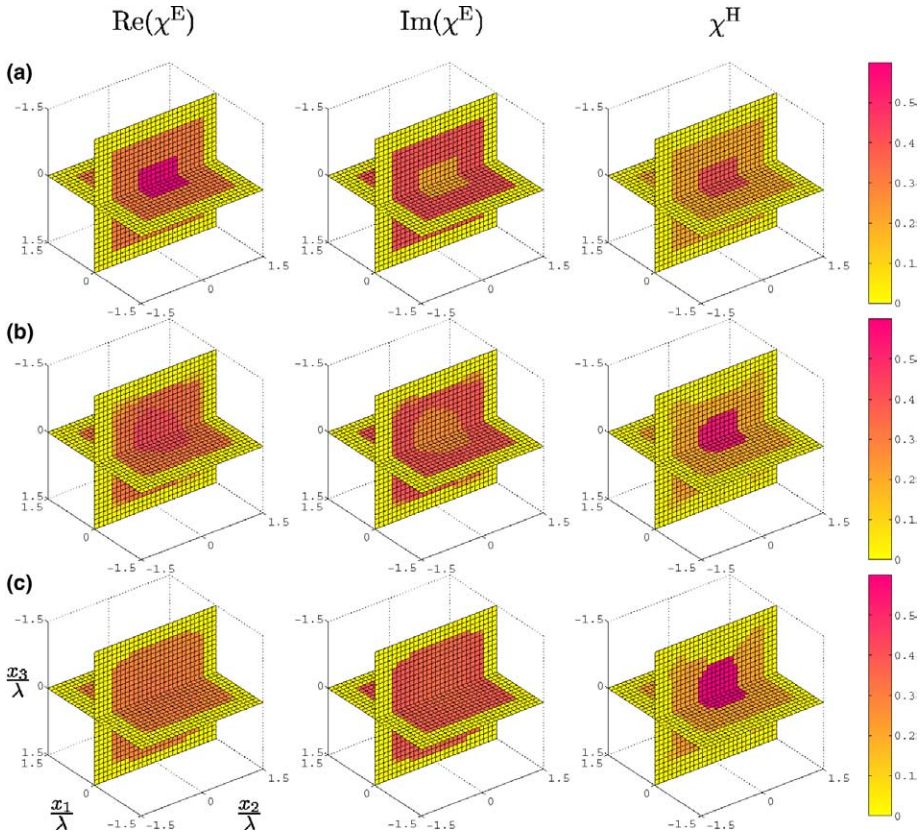

Fig. 10. Configuration of Fig. 4. The exact profiles (a), the reconstructed profiles from simulated data with 5% noise (b) and 10% noise (c).

and magnetic contrast distributions at $x_1 = 0$ and at $x_3 = 0$. The real part of the electric contrast is given in the left plots, its imaginary part is given in the middle plots and the magnetic contrast is given in the right plots of Fig. 10(a).

The simulated data are generated using 30 sources distributed uniformly on three rings (10 sources on each ring) with center at $(0, 0, -0.75\lambda)$, $(0, 0, 0)$ and $(0, 0, 0.75\lambda)$. The radius of these rings is 3λ. The measurement data (the vector scattered electric and magnetic fields) are measured on 90 receivers also distributed uniformly on the same three rings as the rings contain the sources. We have 30 receivers per ring. Hence, the total data points amount to 30×90. It should be noted, since the unknown scatterers have both electric and magnetic contrasts, that this example is more complicated than the previous one. Hence, after generation of this data set, in order to see whether we have enough data points in order to obtain reconstruction results with acceptable resolution, we added 5% and 10% pseudo-random noise of the maximum amplitude of all excitation data per component according to (74) and (75).

In the inversion, we assume that the unknown scatterers are contained in the object domain D with size of 3λ by 3λ by 3λ. This test domain is subdivided into smaller rectangular domain of 30 by 30 by 30. Again, we note that the problem is underdetermined since we have $6 \times 30 \times 90$ data points and $2 \times 30 \times 30 \times 30$ contrast unknowns. The reconstructed results after 1024 iterations of our numerical algorithm from simulated data with 5% noise are given in Fig. 10(b). From the results presented in the plots in Fig. 10(b), we observe that the size, shape and the amplitude of the contrasts (permittivity, conductivity and permeability) of the cubes O_1 and O_2 are very well reconstructed.

The reconstruction results of the data with higher level noise, namely 10% noise, are given in Fig. 10(c). After 1024 iterations the error in electric contrast and magnetic contrast are reduced to $\mathrm{ERR}^{\mathrm{E}} = 0.07$ and $\mathrm{ERR}^{\mathrm{H}} = 0.21$. The errors in contrast as function of iterations are given in Fig. 11. We still observe excellent reconstructed size, shape and amplitude of the large cube. On the other hand, we observe that we can detect its presence only from the reconstructed result of the magnetic contrast χ^{H}, see the right plot in Fig. 10(c). Furthermore, the reconstructed magnetic contrast of the cube O_2 is overestimated (it is $\chi^{\mathrm{H}} = 0.5$ instead of $\chi^{\mathrm{H}} = 0.4$). These last drawbacks are caused by the presence of high level noise (10% noise of the maximum amplitude of the data per component of the scattered fields). We expect that by adding more data points, these negative effect of noise can be reduced.

We further also note that the reconstruction in the domain $x_3 \leqslant -\lambda$ and $x_3 \geqslant \lambda$ is inferior to the one in the domain of $-\lambda \leqslant x_3 \leqslant \lambda$, see Figs. 10(b) and (c). This is simply caused by the absence of the sources and receivers at those x_3 levels.

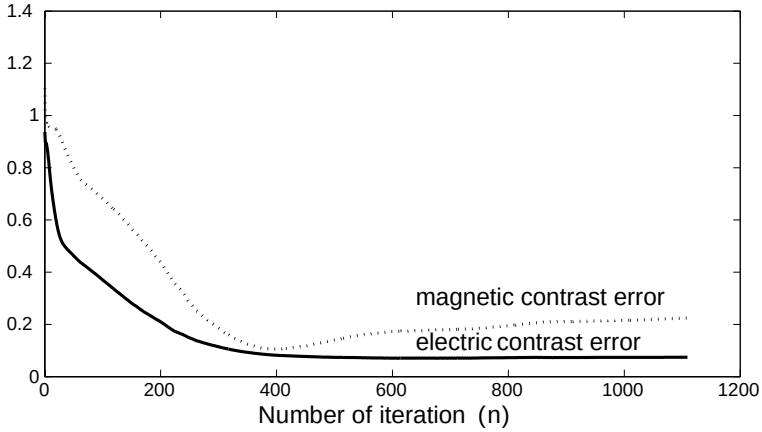

Fig. 11. The error in electric contrast $\mathrm{ERR}^{\mathrm{E}}$ (solid line) and magnetic contrast $\mathrm{ERR}^{\mathrm{H}}$ (dashed line) as function of iteration n of the scatterers containing electric and magnetic contrast with 10% noise.

5. Conclusion

In this paper we have presented a full vectorial three-dimensional nonlinear inversion algorithm with the ability to reconstruct unknown objects which might have the electric (permittivity and conductivity) and/or the magnetic (permeability) contrast. Since this type of inverse problem involves a large number of unknowns, it should be solved as efficiently as possible. To that end we have employed the so-called Multiplicative Regularized Contrast Source Inversion which has the following advantages above other full nonlinear inversion methods known in the literature: (1) It does not solve a full forward problem in each iterative step, in fact the computational complexity of each iteration of this algorithm is equal to number of unknowns times one iteration of the computational complexity of linear conjugate gradient method. (2) It uses a multiplicative constraint, hence the weighting parameter of the regularization factor used in this algorithm is determined automatically. Numerical testings have illustrated that the presence numerical algorithm is able to solve this full vectorial three-dimensional problem with electric and magnetic contrasts, both in the forward and in the inverse scattering problem. When the measured scattered field in a sufficient number of data points are sensitive to variations in the contrast of the object, we are able to construct these variations. In practice, e.g., for a dielectric object, it means that we can reconstruct objects up to $k_b d\chi_{\max} \approx 25$ where $\chi_{\max}$ denotes the maximum amplitude of the contrast and $d_{\max}$ denotes the maximum diameter of the contrasting object.

Appendix A. Discretization procedure

Before discussing the discretization procedure of the integral equations for the electric and magnetic contrast sources in (10) and (11), we first write them as

$$\chi^{\mathrm{E}} E^{\mathrm{inc}}_{\kappa} = w^{\mathrm{E}}_{\kappa} - \chi^{\mathrm{E}}(k_b^2 A^{\mathrm{E}}_{\kappa} + B^{\mathrm{E}}_{\kappa}), \tag{A.1}$$

$$\chi^{\mathrm{H}} Z_b H^{\mathrm{inc}}_{\kappa} = w^{\mathrm{H}}_{\kappa} - \chi^{\mathrm{H}}(k_b^2 A^{\mathrm{H}}_{\kappa} + B^{\mathrm{H}}_{\kappa}), \quad \kappa \in \{1,2,3\}, \tag{A.2}$$

where the vectors B^{E}_{κ} and B^{H}_{κ} are given by

$$B^{\mathrm{E}}_{\kappa} = \partial_{\kappa} \sum_{\nu=1}^{3} \partial_{\nu} A^{\{\mathrm{E,H}\}}_{\nu} + \frac{\mathrm{i}\omega\mu_b}{Z_b} \sum_{\eta,\xi=1}^{3} \epsilon_{\kappa,\eta,\xi} \partial_{\eta} A^{\mathrm{H}}_{\xi}, \tag{A.3}$$

$$B^{\mathrm{H}}_{\kappa} = Z_b \sigma'_b \sum_{\eta,\xi=1}^{3} \epsilon_{\kappa,\eta,\xi} \partial_{\eta} A^{\mathrm{E}}_{\xi} + \partial_{\kappa} \sum_{\nu=1}^{3} \partial_{\nu} A^{\{\mathrm{E,H}\}}_{\nu}, \quad \kappa \in \{1,2,3\}, \tag{A.4}$$

where $\epsilon_{\kappa,\eta,\xi}$ denotes the Levi–Civita tensor. [1] The normalized vector potentials A^{E}_{κ} and A^{H}_{κ} are given by

$$A^{\{\mathrm{E,H}\}}_{\kappa}(\boldsymbol{x}) = \int_D g(\boldsymbol{x}-\boldsymbol{x}') w^{\{\mathrm{E,H}\}}_{\kappa}(\boldsymbol{x}')\, \mathrm{d}v(\boldsymbol{x}'). \tag{A.5}$$

We assume that the domain D is a rectangular domain with boundaries along the x_1, x_2, and x_3 directions as shown in Fig. 12. We discretize the domain D uniformly in rectangular subdomains of dimension $\Delta x_1 \times \Delta x_2 \times \Delta x_3$ with center points

[1] The values of the Levi–Civita tensor are given by $\epsilon_{1,2,3} = \epsilon_{2,3,1} = \epsilon_{3,1,2} = 1$, $\epsilon_{3,2,1} = \epsilon_{2,1,3} = \epsilon_{1,3,2} = 1$ and all other components are zero.

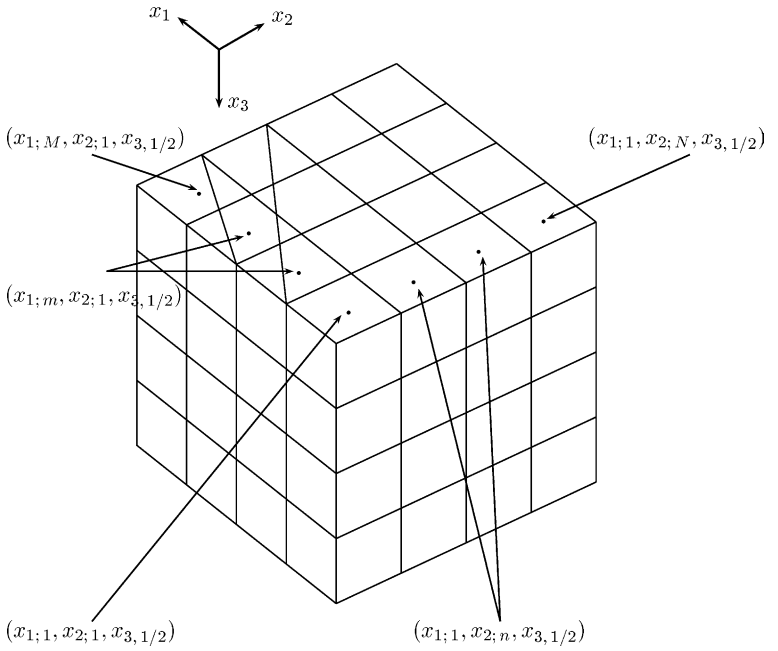

Fig. 12. The spatial discretization grid of the computational domain D.

$$\begin{aligned} x_{1;m} &= x_{1;1/2} + (m-1/2)\Delta x_1, \quad m = 1,\ldots,M,\\ x_{2;n} &= x_{2;1/2} + (n-1/2)\Delta x_2, \quad n = 1,\ldots,N,\\ x_{3;p} &= x_{3;1/2} + (p-1/2)\Delta x_3, \quad p = 1,\ldots,P, \end{aligned} \tag{A.6}$$

in which $x_{\kappa;1/2}$ denotes the lower bound in the x_κ-direction. In each subdomain, we assume the material contrast χ to be constant, with value the same as the value of χ at the center point

$$\chi^{\mathrm{E,H}}_{m,n,p} = \chi^{\mathrm{E,H}}(x_{1;m}, x_{2;n}, x_{3;p}). \tag{A.7}$$

Similar definitions for the vectorial field quantities are used. In view of the presence of spatial differentiations in (A.3) and (A.4), the boundary of the domain D is chosen to be lied completely outside the scattering objects, where the contrast quantities vanish. Then (A.1) and (A.2) are discretized as follows:

$$\chi^{\mathrm{E}}_{m,n,p} E^{\mathrm{inc}}_{\kappa;m,n,p} = w^{\mathrm{E}}_{\kappa;m,n,p} - \chi^{\mathrm{E}}_{m,n,p}(k_{\mathrm{b}}^2 A^{\mathrm{E}}_{\kappa;m,n,p} + B^{\mathrm{E}}_{\kappa;m,n,p}), \tag{A.8}$$

$$\chi^{\mathrm{H}}_{m,n,p} Z_{\mathrm{b}} H^{\mathrm{inc}}_{\kappa;m,n,p} = w^{\mathrm{H}}_{\kappa;m,n,p} - \chi^{\mathrm{H}}_{m,n,p}(k_{\mathrm{b}}^2 A^{\mathrm{H}}_{\kappa;m,n,p} + B^{\mathrm{H}}_{\kappa;m,n,p}), \tag{A.9}$$

for $m = 1,\ldots,M$, $n = 1,\ldots,N$ and $p = 1,\ldots,P$. The vector functions B^{E}_κ and B^{H}_κ in (A.3) adn (A.4) are computed with finite difference rules [1]. The results are given by

$$\begin{aligned} B^{\mathrm{E}}_{1;m,n,p} = {} & \frac{A^{\mathrm{E}}_{1;m-1,n,p} - 2A^{\mathrm{E}}_{1;m,n,p} + A^{\mathrm{E}}_{1;m+1,n,p}}{\Delta x_1^2} + \frac{A^{\mathrm{E}}_{2;m-1,n-1,p} - A^{\mathrm{E}}_{2;m-1,n+1,p} - A^{\mathrm{E}}_{2;m+1,n-1,p} + A^{\mathrm{E}}_{2;m+1,n+1,p}}{4\Delta x_1 \Delta x_2}\\ & + \frac{A^{\mathrm{E}}_{3;m-1,n,p-1} - A^{\mathrm{E}}_{3;m-1,n,p+1} - A^{\mathrm{E}}_{3;m+1,n,p-1} + A^{\mathrm{E}}_{3;m+1,n,p+1}}{4\Delta x_1 \Delta x_3}\\ & + \frac{\mathrm{i}\omega\mu_{\mathrm{b}}}{Z_{\mathrm{b}}}\left(\frac{A^{\mathrm{H}}_{3;m,n+1,p} - A^{\mathrm{H}}_{3;m,n-1,p}}{2\Delta x_2} - \frac{A^{\mathrm{H}}_{2;m,n,p+1} - A^{\mathrm{H}}_{2;m,n,p-1}}{2\Delta x_3}\right), \end{aligned} \tag{A.10}$$

$$B^{\mathrm{H}}_{1;m,n,p} = \frac{A^{\mathrm{H}}_{1;m-1,n,p} - 2A^{\mathrm{H}}_{1;m,n,p} + A^{\mathrm{H}}_{1;m+1,n,p}}{\Delta x_1^2} + \frac{A^{\mathrm{H}}_{2;m-1,n-1,p} - A^{\mathrm{H}}_{2;m-1,n+1,p} - A^{\mathrm{H}}_{2;m+1,n-1,p} + A^{\mathrm{H}}_{2;m+1,n+1,p}}{4\Delta x_1 \Delta x_2} + \frac{A^{\mathrm{H}}_{3;m-1,n,p-1} - A^{\mathrm{H}}_{3;m-1,n,p+1} - A^{\mathrm{H}}_{3;m+1,n,p-1} + A^{\mathrm{H}}_{3;m+1,n,p+1}}{4\Delta x_1 \Delta x_3} + Z_{\mathrm{b}}\sigma'_{\mathrm{b}}\left(\frac{A^{\mathrm{E}}_{3;m,n+1,p} - A^{\mathrm{E}}_{3;m,n-1,p}}{2\Delta x_2} - \frac{A^{\mathrm{E}}_{2;m,n,p+1} - A^{\mathrm{E}}_{2;m,n,p-1}}{2\Delta x_3} \right), \tag{A.11}$$

where $B^{\mathrm{E}}_{2;m,n,p}$, $B^{\mathrm{E}}_{3;m,n,p}$, $B^{\mathrm{H}}_{2;m,n,p}$ and $B^{\mathrm{H}}_{3;m,n,p}$ are obtained by permutations.

Next, we have to replace the continuous representation of the normalized vector potentials $A^{\{\mathrm{E,H}\}}_{\kappa}(\boldsymbol{x})$ in (A.5) by discrete ones. In order to cope with the singularity of the Green function, we apply the weakening procedure to the normalized vector potentials. After the weakening procedure, we compute the integral over D in the normalized vector potentials numerically using a midpoint rule. We then arrive at

$$A^{\{\mathrm{E,H}\}}_{\kappa;m,n,p} = \Delta x_1 \Delta x_2 \Delta x_3 \sum_{m'=1}^{M} \sum_{n'=1}^{N} \sum_{p'=1}^{P} \mathscr{G}_{m-m',n-n',p-p'} w^{\{\mathrm{E,H}\}}_{\kappa;m',n',p'}, \tag{A.12}$$

for $m = 0, \ldots, M+1$, $n = 0, \ldots, N+1$, and $p = 0, \ldots, P+1$, where

$$\mathscr{G}_{m,n,p} = \begin{cases} \frac{[1 - \frac{1}{2}\mathrm{i}k_{\mathrm{b}}\Delta x]\exp(\frac{1}{2}\mathrm{i}k_{\mathrm{b}}\Delta x) - 1}{\frac{1}{6}\pi k_{\mathrm{b}}^2 \Delta x^3}, & m,n,p = 0, \\ g(x_{1;m}, x_{2;n}, x_{3;p}), & \text{otherwise}, \end{cases} \tag{A.13}$$

in which $\Delta x = \min(\Delta x_1, \Delta x_2, \Delta x_3)$. Note that $A^{\{\mathrm{E,H}\}}_{\kappa;m,n,p}$ are discrete convolutions in m', n', and p' and can efficiently be computed by three-dimensional FFT routines [23]. Finally, we remark that this weakening of the singularity is different from the technique used by van Bladel [11], where the spatial differentiations are acting on the Green function directly, while we compute first the normalized vector potential $A^{\{\mathrm{E,H}\}}_{\kappa}$, in which the Green function has been weakened by taking its spherical mean [26], and subsequently the differentiations are carried out numerically on the normalized vector potential $A^{\{\mathrm{E,H}\}}_{\kappa}$. This technique has proven [2,6] to yield an efficient, stable, and accurate algorithm.

Appendix B. Adjoint operators

The adjoint operators of the domain integral operators on D in (16) and (18) are defined through the relationship

$$\left\langle \begin{bmatrix} \boldsymbol{r}^{\mathrm{E}} \\ \boldsymbol{r}^{\mathrm{H}} \end{bmatrix}, \begin{bmatrix} \mathscr{L}^{\mathrm{EE}}_D \boldsymbol{w}^{\mathrm{E}} + \mathscr{L}^{\mathrm{EH}}_D \boldsymbol{w}^{\mathrm{H}} \\ \mathscr{L}^{\mathrm{HE}}_D \boldsymbol{w}^{\mathrm{E}} + \mathscr{L}^{\mathrm{HH}}_D \boldsymbol{w}^{\mathrm{H}} \end{bmatrix} \right\rangle_D = \left\langle \begin{bmatrix} \mathscr{L}^{\mathrm{EE}*}_D \boldsymbol{r}^{\mathrm{E}} + \mathscr{L}^{\mathrm{HE}*}_D \boldsymbol{r}^{\mathrm{H}} \\ \mathscr{L}^{\mathrm{EH}*}_D \boldsymbol{r}^{\mathrm{E}} + \mathscr{L}^{\mathrm{HH}*}_D \boldsymbol{r}^{\mathrm{H}} \end{bmatrix}, \begin{bmatrix} \boldsymbol{w}^{\mathrm{E}} \\ \boldsymbol{w}^{\mathrm{H}} \end{bmatrix} \right\rangle_D, \tag{B.1}$$

where $[\boldsymbol{w}^{\mathrm{E}} \ \ \boldsymbol{w}^{\mathrm{H}}]$ and $[\boldsymbol{r}^{\mathrm{E}} \ \ \boldsymbol{r}^{\mathrm{H}}]$ are both in the same vector space. Substituting (18) and (19) with (A.10)–(A.13) in the left-hand side of (B.1), and interchanging the various summations the adjoint operators are recognized as

$$(\mathscr{L}^{\mathrm{EE}*}_D \boldsymbol{r}^{\mathrm{E}} + \mathscr{L}^{\mathrm{HE}*}_D \boldsymbol{r}^{\mathrm{H}})_{\kappa;m,n,p} = r^{\mathrm{E}}_{\kappa;m,n,p} - C^{\mathrm{E}}_{\kappa;m,n,p}, \tag{B.2}$$

$$(\mathscr{L}^{\mathrm{EH}*}_D \boldsymbol{r}^{\mathrm{E}} + \mathscr{L}^{\mathrm{HH}*}_D \boldsymbol{r}^{\mathrm{H}})_{\kappa;m,n,p} = r^{\mathrm{H}}_{\kappa;m,n,p} - C^{\mathrm{H}}_{\kappa;m,n,p} \tag{B.3}$$

for $m = 1, \ldots, M$, $n = 1, \ldots, N$, $p = 1, \ldots, P$ and where

$$C^{\{\mathrm{E,H}\}}_{\kappa;m,n,p} = \Delta x_1 \Delta x_2 \Delta x_3 \sum_{m'=0}^{M+1} \sum_{n'=0}^{N+1} \sum_{p'=0}^{P+1} \overline{\mathscr{G}}_{m-m',n-n',p-p'} F^{\{\mathrm{E,H}\}}_{\kappa;m',n',p'}, \tag{B.4}$$

in which

$$\begin{aligned} F^{\mathrm{E}}_{1;m,n,p} = {} & \overline{k_{\mathrm{b}}^2} s^{\mathrm{E}}_{1;m,n,p} + \frac{s^{\mathrm{E}}_{1;m-1,n,p} - 2s^{\mathrm{E}}_{1;m,n,p} + s^{\mathrm{E}}_{1;m+1,n,p}}{\Delta x_1^2} \\ & + \frac{s^{\mathrm{E}}_{2;m-1,n-1,p} - s^{\mathrm{E}}_{2;m-1,n+1,p} - s^{\mathrm{E}}_{2;m+1,n-1,p} + s^{\mathrm{E}}_{2;m+1,n+1,p}}{4\Delta x_1 \Delta x_2} \\ & + \frac{s^{\mathrm{E}}_{3;m-1,n,p-1} - s^{\mathrm{E}}_{3;m-1,n,p+1} - s^{\mathrm{E}}_{3;m+1,n,p-1} + s^{\mathrm{E}}_{3;m+1,n,p+1}}{4\Delta x_1 \Delta x_3} \\ & + \overline{Z_{\mathrm{b}} \sigma'_{\mathrm{b}}} \left(\frac{s^{\mathrm{H}}_{3;m,n+1,p} - s^{\mathrm{H}}_{3;m,n-1,p}}{2\Delta x_2} - \frac{s^{\mathrm{H}}_{2;m,n,p+1} - s^{\mathrm{H}}_{2;m,n,p-1}}{2\Delta x_3} \right), \end{aligned} \tag{B.5}$$

$$\begin{aligned} F^{\mathrm{H}}_{1;m,n,p} = {} & \overline{k_{\mathrm{b}}^2} s^{\mathrm{H}}_{1;m,n,p} + \frac{s^{\mathrm{H}}_{1;m-1,n,p} - 2s^{\mathrm{H}}_{1;m,n,p} + s^{\mathrm{H}}_{1;m+1,n,p}}{\Delta x_1^2} + \frac{s^{\mathrm{H}}_{2;m-1,n-1,p} - s^{\mathrm{H}}_{2;m-1,n+1,p} - s^{\mathrm{H}}_{2;m+1,n-1,p} + s^{\mathrm{H}}_{2;m+1,n+1,p}}{4\Delta x_1 \Delta x_2} \\ & + \frac{s^{\mathrm{H}}_{3;m-1,n,p-1} - s^{\mathrm{H}}_{3;m-1,n,p+1} - s^{\mathrm{H}}_{3;m+1,n,p-1} + s^{\mathrm{H}}_{3;m+1,n,p+1}}{4\Delta x_1 \Delta x_3} \\ & + \frac{\overline{\mathrm{i}\omega\mu_{\mathrm{b}}}}{\overline{Z_{\mathrm{b}}}} \left(\frac{s^{\mathrm{E}}_{3;m,n+1,p} - s^{\mathrm{E}}_{3;m,n-1,p}}{2\Delta x_2} - \frac{s^{\mathrm{E}}_{2;m,n,p+1} - s^{\mathrm{E}}_{2;m,n,p-1}}{2\Delta x_3} \right), \end{aligned} \tag{B.6}$$

where $F^{\mathrm{E}}_{2;m,n,p}$, $F^{\mathrm{E}}_{3;m,n,p}$, $F^{\mathrm{H}}_{2;m,n,p}$ and $F^{\mathrm{H}}_{3;m,n,p}$ are obtained by permutations and in which

$$s^{\{\mathrm{E,H}\}}_{\kappa;m,n,p+1} = \overline{\chi}^{\{\mathrm{E,H}\}}_{m,n,p} r^{\{\mathrm{E,H}\}}_{\kappa;m,n,p+1}. \tag{B.7}$$

Since according to (B.4) m' runs from 0 to $M+1$, n' runs from 0 to $N+1$, and p' runs from 0 to $P+1$, we set in Eqs. (B.5) and (B.6)

$$\begin{aligned} & r^{\{\mathrm{E,H}\}}_{\kappa;m,n,p} = 0, \quad m = -1, 0, M+1, M+2 \quad \forall n \forall p, \\ & r^{\{\mathrm{E,H}\}}_{\kappa;m,n,p} = 0, \quad n = -1, 0, N+1, N+2 \quad \forall m \forall p, \\ & r^{\{\mathrm{E,H}\}}_{\kappa;m,n,p} = 0, \quad p = -1, 0, P+1, P+2, \quad \forall m \forall n. \end{aligned} \tag{B.8}$$

Note that $C^{\{\mathrm{E,H}\}}_{\kappa;m,n,p}$ is discrete convolution in m', n', and p' and these convolutions can be also computed efficiently by three-dimensional FFT routines [23].

Appendix C. Data operator

Since the integral operators in (14) and (15) contain no singular point, these operators can directly be discretized. After calculating the integral using midpoint rule, we arrive at

$$E^{\mathrm{sct}}_{\kappa}(\boldsymbol{x}) = k_{\mathrm{b}}^2 A^{\mathrm{E}}_{\kappa}(\boldsymbol{x}) + B^{\mathrm{E}}_{\kappa}(\boldsymbol{x}), \tag{C.1}$$

$$Z_{\mathrm{b}} H^{\mathrm{sct}}_{\kappa}(\boldsymbol{x}) = k_{\mathrm{b}}^2 A^{\mathrm{H}}_{\kappa}(\boldsymbol{x}) + B^{\mathrm{H}}_{\kappa}(\boldsymbol{x}), \quad \kappa \in \{1, 2, 3\}, \tag{C.2}$$

where the vectors B_κ^{E} and B_κ^{H} are given by

$$B_\kappa^{\mathrm{E}}(x_1,x_2,x_3) = \partial_\kappa \sum_{v=1}^{3} \partial_v A_v^{\mathrm{E}}(x_1,x_2,x_3) + \frac{\mathrm{i}\omega\mu_{\mathrm{b}}}{Z_{\mathrm{b}}} \sum_{v,\xi=1}^{3} \epsilon_{\kappa,v,\xi}\partial_v A_\xi^{\mathrm{H}}(x_1,x_2,x_3), \tag{C.3}$$

$$B_\kappa^{\mathrm{H}}(x_1,x_2,x_3) = Z_{\mathrm{b}}\sigma'_{\mathrm{b}} \sum_{v,\xi=1}^{3} \epsilon_{\kappa,v,\xi}\partial_v A_\xi^{\mathrm{E}}(x_1,x_2,x_3) + \partial_\kappa \sum_{v=1}^{3} \partial_v A_v^{\mathrm{H}}(x_1,x_2,x_3), \tag{C.4}$$

in which

$$A_\kappa^{\{\mathrm{E,H}\}}(x_1,x_2,x_3) = \Delta x_1\Delta x_2\Delta x_3 \sum_{m=1}^{M}\sum_{n=1}^{N}\sum_{p=1}^{P} g(x_1-x_{1,m},x_2-x_{2,n},x_3-x_{3,p}) w_{v;m,n,p}^{\{\mathrm{E,H}\}}. \tag{C.5}$$

For the formulation of our inversion algorithm, we also need the adjoint operators of the integral representations on S. The adjoint operators of the operator in the data equations in (52) are defined through the relationship

$$\left\langle \begin{bmatrix} \boldsymbol{\rho}^{\mathrm{E}} \\ \boldsymbol{\rho}^{\mathrm{H}} \end{bmatrix}, \begin{bmatrix} \mathscr{K}_S^{\mathrm{EE}}\boldsymbol{w}^{\mathrm{E}} + \mathscr{L}_S^{\mathrm{EH}}\boldsymbol{w}^{\mathrm{H}} \\ \mathscr{K}_S^{\mathrm{HE}}\boldsymbol{w}^{\mathrm{E}} + \mathscr{L}_S^{\mathrm{HH}}\boldsymbol{w}^{\mathrm{H}} \end{bmatrix} \right\rangle_S = \left\langle \begin{bmatrix} \mathscr{K}_S^{\mathrm{EE}*}\boldsymbol{\rho}^{\mathrm{E}} + \mathscr{K}_S^{\mathrm{HE}*}\boldsymbol{\rho}^{\mathrm{H}} \\ \mathscr{K}_S^{\mathrm{EH}*}\boldsymbol{\rho}^{\mathrm{E}} + \mathscr{K}_S^{\mathrm{HH}*}\boldsymbol{\rho}^{\mathrm{H}} \end{bmatrix}, \begin{bmatrix} \boldsymbol{w}^{\mathrm{E}} \\ \boldsymbol{w}^{\mathrm{H}} \end{bmatrix} \right\rangle_D, \tag{C.6}$$

where $[\boldsymbol{w}^{\mathrm{E}}\ \ \boldsymbol{w}^{\mathrm{H}}]$ are vector quantities on D and $[\boldsymbol{\rho}^{\mathrm{E}}\ \ \boldsymbol{\rho}^{\mathrm{H}}]$ are vector quantities on S. Substituting the right-hand side of (C.1) and (C.2) with (C.3)–(C.5) in the left-hand side of (C.6), and interchanging the various summations the adjoint operators are recognized as

$$\left(\mathscr{K}_S^{\mathrm{EE}*}\boldsymbol{\rho}^{\mathrm{E}} + \mathscr{K}_S^{\mathrm{HE}*}\boldsymbol{\rho}^{\mathrm{H}}\right)_{\kappa;m,n,p} = C_{\kappa;m,n,p}^{\mathrm{E}}, \tag{C.7}$$

$$\left(\mathscr{K}_S^{\mathrm{EH}*}\boldsymbol{\rho}^{\mathrm{E}} + \mathscr{K}_S^{\mathrm{HH}*}\boldsymbol{\rho}^{\mathrm{H}}\right)_{\kappa;m,n,p} = C_{\kappa;m,n,p}^{\mathrm{H}} \tag{C.8}$$

for $m = 1,\ldots,M$, $n = 1,\ldots,N$, $p = 1,\ldots,P$ and where

$$\begin{aligned} C_{\kappa;m,n,p}^{\mathrm{E}} = & \sum_{\forall \boldsymbol{x}\in S} \partial_\kappa \sum_{v=1}^{3} \partial_v \overline{g}(x_1-x_{1,m},x_2-x_{2,n},x_3-x_{3,p})\rho_v^{\mathrm{E}}(x_1,x_2,x_3) \\ & + \sum_{\forall \boldsymbol{x}\in S} \frac{\mathrm{i}\omega\mu_{\mathrm{b}}}{Z_{\mathrm{b}}} \sum_{v,\xi=1}^{3} \epsilon_{\kappa,v,\xi}\partial_v \overline{g}(x_1-x_{1,m},x_2-x_{2,n},x_3-x_{3,p})\rho_\xi^{\mathrm{E}}(x_1,x_2,x_3), \end{aligned} \tag{C.9}$$

$$\begin{aligned} C_{\kappa;m,n,p}^{\mathrm{H}} = & \sum_{\forall \boldsymbol{x}\in S} \partial_\kappa \sum_{v=1}^{3} \partial_v \overline{g}(x_1-x_{1,m},x_2-x_{2,n},x_3-x_{3,p})\rho_v^{\mathrm{H}}(x_1,x_2,x_3) \\ & + \sum_{\forall \boldsymbol{x}\in S} Z_{\mathrm{b}}\sigma'_{\mathrm{b}} \sum_{v,\xi=1}^{3} \epsilon_{\kappa,v,\xi}\partial_v \overline{g}(x_1-x_{1,m},x_2-x_{2,n},x_3-x_{3,p})\rho_v^{\mathrm{E}}(x_1,x_2,x_3). \end{aligned} \tag{C.10}$$

References

[1] M. Abramowitz, I.A. Stegun, in: Handbook of Mathematical Functions, vol. 884, Dover, New York, 1970.
[2] A. Abubakar, P.M. van den Berg, Three dimensional nonlinear inversion in cross-well electrode logging, Radio Science 33 (4) (1998) 989–1004.

[3] A. Abubakar, P.M. van den Berg, Nonlinear inversion in electrode logging in a highly deviated formation with invasion using an oblique coordinate system, IEEE Transactions on Geoscience and Remote Sensing 38 (2000) 25–39.
[4] A. Abubakar, P.M. van den Berg, Three-dimensional inverse scattering applied to cross-well induction sensors, invited paper, Special Issue on Computational Wave Issues in Remote Sensing, Imaging, Target Identification, Propagation and Inverse Scattering in: IEEE Transactions on Geoscience and Remote Sensing, vol. 38, 2000, pp. 1669–1681.
[5] A. Abubakar, P.M. van den Berg, B.J. Kooij, A conjugate gradient contrast source technique for 3D profile inversion, IEICE Transactions on Electronics E 83-C (2000) 1864–1877.
[6] A. Abubakar, three-dimensional non-linear inversion of electrical conductivity, Ph.D. Thesis, Delft University Press, Delft, 2000, 258p.
[7] A. Abubakar, P.M. van den Berg, Nonlinear inversion of the electrode logging measurements in a deviated well, Geophysics 66 (2001) 110–124.
[8] A. Abubakar, P.M. van den Berg, Total variation as a multiplicative constraint for solving inverse problems, IEEE Transactions on Image Processing 10 (2001) 1384–1392.
[9] A. Abubakar, P.M. van den Berg, S.Y. Semenov, Two- and three-dimensional algorithms for microwave imaging and inverse scattering, Journal of Electromagnetic Waves and Applications 17 (2) (2003) 209–231.
[10] S. Barkeshli, R.G. Lautzenheiser, An iterative method for inverse scattering problems based on an exact gradient search, Radio Science 29 (1994) 1119–1130.
[11] J. van Bladel, Singular Electromagnetic Fields and Sources, Clarendon Press, Oxford, 1991, 232p.
[12] R.F. Bloemenkamp, A. Abubakar, P.M. van den Berg, Inversion of experimental multi-frequency data using the Contrast Source Inversion method, Inverse Problem 17 (2001) 1611–1622.
[13] W.C. Chew, Y.M. Wang, Reconstruction of two-dimensional permittivity distribution using the distorted Born iterative method, IEEE Transactions on Medical Imaging 9 (1990) 218–225.
[14] A. Franchois, C. Pichot, Microwave imaging – Complex permittivity reconstruction with Levenberg–Marquardt method, IEEE Transactions on Antennas and Propagation 45 (1997) 203–215.
[15] T.M. Habashy, R.J. Mitra, On some inverse methods in electromagnetics, Journal of Electromagnetic Waves and Applications 1 (1987) 25–58.
[16] T.M. Habashy, M.L. Oristaglio, A.T. de Hoop, Simultaneous nonlinear reconstruction of two-dimensional permittivity and conductivity, Radio Science 29 (1994) 1101–1118.
[17] A.T. de Hoop, Handbook of Radiation and Scattering of Waves, Academic Press, Delft, 1995.
[18] T. Isernia, V. Pascazio, R. Pierri, On the local minima in a tomographic imaging technique, IEEE Transactions on Geoscience and Remote Sensing 39 (2001) 1596–1607.
[19] R.E. Kleinman, P.M. van den Berg, A modified gradient method for two-dimensional problems in tomography, Journal of Computational and Applied Mathematics 42 (1992) 17–35.
[20] Q.H. Liu, W.C. Chew, Applications of the CG-FFHT method with an improved FHT algorithm, Radio Science 29 (1994) 1009–1022.
[21] P.E. Wannamaker, G.W. Hohmann, W.A. SanFilipo, Electromagnetic modeling of three-dimensional bodies in layered earth using integral equations, Geophysics 49 (1984) 60–74.
[22] M. Oristaglio, B. Spies, Three Dimensional Electromagnetics, Society of Exploration Geophysics, Tulsa, OK, 1999, 709pp.
[23] W.H. Press, S.A. Teukolsky, W.T. Vetterling, B.P. Flannery, Numerical Recipes in Fortran: The Art of Scientific Computing, Cambridge University Press, New York, 1992.
[24] I.T. Rekanos, A. Raisanen, Microwave imaging in the time domain of buried multiple scatterers by using an FDTD-based optimization technique, IEEE Transactions on Magnetics 39 (3) (2003) 1381–1384.
[25] I.T. Rekanos, Time-domain inverse scattering using Lagrange multipliers: an iterative FDTD-based optimization technique, Journal of Electromagnetic Waves and Applications 17 (2) (2003) 271–289.
[26] J.H. Richmond, Scattering by a dielectric cylinder of arbitrary cross section shape, IEEE Transactions on Antennas and Propagation 13 (1965) 334–341.
[27] C. Torres-Verdin, T.M. Habashy, A two-step linear inversion of two-dimensional electrical conductivity, IEEE Transactions on Antennas and Propagation 43 (1995) 405–415.
[28] M. Gustafsson, S. He, An optimization approach to two-dimensional time domain electromagnetic inverse problems, Radio Science 35 (2000) 525–536.
[29] P.M. van den Berg, R.E. Kleinman, A contrast source inversion method, Inverse Problems 13 (1997) 1607–1620.
[30] P.M. van den Berg, A. Abubakar, Contrast source inversion method: state of art, Progress in Electromagnetic Research 34 (2001) 189–218.
[31] P.M. van den Berg, A. Abubakar, J.T. Fokkema, Multiplicative regularization for contrast profile inversion, Radio Science 38 (2) (2003) 8022, doi:10.1029/2001RS002555.
[32] M.S. Zhdanov, V.V. Chernyak, An automated method of solving the two-dimensional inverse problem of electromagnetic induction within the earth, Transactions (Doklady) USSR Academy of Sciences, Earth Science Sections 296 (5) (1987) 59–63.

[33] M.S. Zhdanov, G. Hursan, 3D electromagnetic inversion based on quasi-analytical approximation, Inverse Problems 16 (2000) 1297–1322.
[34] M.S. Zhdanov, P.E. Wannamaker, in: Three-Dimensional Electromagnetics, Methods in Geochemistry and Geophysics, vol. 35, Elsevier, Amsterdam, 2002, 290pp.
[35] M.S. Zhdanov, in: Geophysical Inverse Theory and Regularization, Methods in Geochemistry and Geophysics, vol. 36, Elsevier, Amsterdam, 2002, 290pp.
[36] Z.Q. Zhang, Q.H. Liu, Two nonlinear inverse methods for electromagnetic induction measurements, IEEE Transactions on Geoscience and Remote Sensing 39 (2001) 1331–1339.
[37] A.P.M. Zwamborn, P.M. van den Berg, The three-dimensional weak form of the conjugate gradient FFT method for solving scattering problems, IEEE Transactions on Microwave Theory and Techniques 40 (1992) 1757–1766.
[38] A.P.M. Zwamborn, P.M. van den Berg, Computation of electromagnetic fields inside strongly objects by the weak-conjugate gradient FFT method, Journal of Optical Society 11 (1994) 1414–1421.